NTNU

Norwegian University of
Science and Technology

Practical Artifact Cancellation for Myoelectric Prosthesis Control

Marthe Sæther

Master of Science in Engineering Cybernetics
Submission date: June 2008
Supervisor: Geir Mathisen, ITK
Co-supervisor: Øyvind Stavdahl, ITK

Norwegian University of Science and Technology
Department of Engineering Cybernetics

Problem Description

Surface electromyograms (sEMG) contain artifacts induced by e.g. sweat, motion and external forces. These artifacts are undesirable because they impair the performance of myoelectric prosthesis control systems.
In earlier work a setup for simultaneous measurements of sEMG on m. biceps brachii, force sensing resistor (FSR) outputs and muscle contraction force using a load cell has been constructed, together with an experiment protocol for data acquisition. In this assessment the setup will be completed, improved and assessed through physical experiments.

1. Give a brief survey of prior art in mathematical models that describe the correspondence between physical movements/forces and the resulting sEMG artifacts.

2. Improve and characterize a prototype sEMG sensor with built-in FSRs that was developed in a previous work.

3. Perform data acquisition according to the predefined protocol.

4. Assess at least two methods for "artifact-free force estimation" based on mathematical models and/or existing "black box" pattern recognition techniques.

Assignment given: 07. January 2008
Supervisor: Geir Mathisen, ITK

Preface

This thesis is submitted in fulfilment of my Master of Science at the Norwegian University of Science and Technology (NTNU), at the Department of Engineering Cybernetics.

For an amputee, the possibility to get a remedy such as a prosthesis can improve quality of life. My believe is that artifact cancellation in myoelectric prosthesis control can contribute to make prostheses more reliable, and increase the degree of acceptance by amputees. I really hope that the work done in this study will be carried further.

There are many people that have helped me both in the work on this thesis, and other parts of my studies.

First of all I would like to thank my advisor Øyvind Stavdahl for his support and constructive feedback. His positiveness, enthusiasm and friendly behaviour have through this year given me much inspiration and motivation.

Anders Fougner has been very kind to let me use his Matlab/Simulink model and programs, being my collaborator at the laboratory and co-advisor.

For me, the mere thought of constructing a sensor, needing to handle a copper bit and multimeter, was quite frightening. The technical staff & the Engineering workshop at the Department of Engineering Cybernetics, have been very helpful with the construction of my prototype sEMG sensor, and patient answering my "stupid" questions.

I would also like to thank Geir Mathisen for being my institute advisor at NTNU, Dennis Lovely for reviewing my fall project and sharing of his relevant literature, and my dad for giving me credit and being understanding when I need it.

Last, but not least, thanks to my best girls; Helle and Marte. These girls have made my life easier and more enjoyable at school. The benefit of having some like-minded to take time off with is even more appreciated.

Trondheim, June 2008

Marthe Sæther

Contents

List of Figures

List of Tables

Nomenclature

CNS Central nervous system

CMRR Common-mode rejection ratio

DAQ Data acquisition

ECG Electrocardiogram

EEG Electroencephalography

EMG Electromyography

EMG Electromyogram

FSR Force sensing resistor

MVC Maximum voluntary contraction

MES Myoelectric signal

MLP Multi-layer perceptron

sEMG Surface Electromyogram

Abstract

Prostheses are artificial body parts that can be used by amputees. Myoelectric prostheses are controlled by so-called surface electromyograms (sEMG) that are acquired on the skin surface of the residual limb. A well-known problem in myoelectric prostheses is motion artifacts, these artifacts cause unwanted behaviour of the prosthesis.

The purpose of this study is to try to cancel the effect motion artifacts have on myoelectric prosthesis control, in order to avoid unsolicited prosthesis behaviour.

The subject of myoelectric prostheses and motion artifacts are outlined in this study, together with the development and characterization of a sensor that can do simultaneous measurements of sEMG and contact forces between a surface electrode and the skin. A protocol has been developed for recording of the different signals in a laboratory. Suitable data sets have been acquired from a test subject, and signal processing and pattern recognition methods have been applied on these data sets to generate muscle force estimates. The pattern recognition methods were linear and quadratic mapping functions, and multi-layer perceptron network.

To achieve better force estimates when motion artifacts are presence, signals from FSRs are taken into consideration together with sEMG signals. A qualitative comparison reveals obvious improvements for the sEMG sensor when FSR measurement is included. The system presently undergoes quantitative assessment of static and dynamic performance.

The final step will hopefully be to integrate FSRs in a real prosthesis socket.

1 Introduction

Development of prosthetic devices has been an issue for a long time, dating all back to wooden legs. The mechanical approach to prosthesis control was initiated in the U.S. Prostheses can be controlled in several ways, myoelectric control is one approach. The concept of myoelectric control was introduced in the 1940s. With the development of semiconductors device technology and the associated decrease in device size and power requirements, this clinical application saw promise, and research and development have since then increased dramatically. (Parker et al., 2004).

Myoelectrical prostheses control the limbs by converting muscle movements from the residual limb to electrical signals. This muscle movements are detected by surface electrodes, so-called myoelectrodes. Figure 1 presents the relationship between normal and myoelectric control systems (the yellow area represents the part of the system that is removed after an amputation).

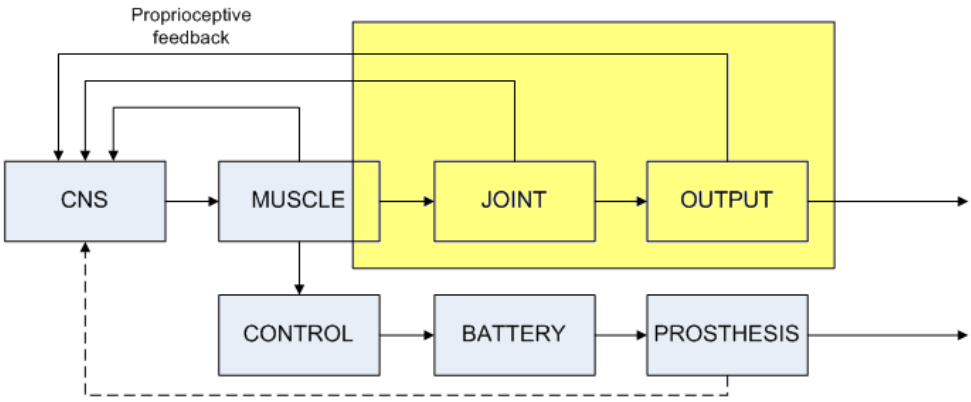

Figure 1: Block diagram illustrating relationship between normal and myoelectric control systems

Electrically powered prostheses with myoelectric control have several advantages over other types of prostheses, but the effect that motion artifacts have on this control strategy is unwanted. Motion artifacts are signal disturbances that arise from movements and varying contact forces at the surface electrode-skin junction (this subject is closer described in Section 2). These artifacts are undesirable because they impair the performance of myoelectric prosthesis control, and are known to cause unsolicited prosthesis behaviour.

Despite these problems, artifact cancellation techniques in myoelectric prosthesis control are extremely limited described in the research literature. Hopefully, the sensor developed in this study can be a contribution in the right direction.

A great effort has been made to record suitable data sets in the laboratory, and the developed signal processing and pattern recognition methods from Fougner (2007) have been applied on these data sets. Their performance has been evaluated, compared and visualized.

The report is outlined as follows:

Section 2: Background theory

Section 3: The aim of the study is presented

Section 4: Presentation of the equipment at the EMG/FES laboratory

Section 5: Discussion of the specific problem and modelling of the surface electrode-skin junction

Section 6: Describes the construction of a device for collecting simultaneous measurements of the myoelectric signal, contact forces and other relevant figures (Sæther (2007)). Improvements and characterization of this sensor will be presented

Section 7: Method description

Section 8: Findings/Results

Section 9: Discussion

Section 10: Conclusion

Section 11: Suggestions for future work

2 Theory

2.1 The human nervous system

This section is cited from Sæther (2007).

Skeletal muscles are controlled by the voluntary nervous system. The central nervous system (CNS) sends short electric pulses, these are called action potentials, via motor neurons (or motoneurons) to the motor end-plates of the muscle fibers. A motor neuron and all muscle fibers it innervates form a separately controllable unit of the muscle. This is called the motor unit. Muscle force is decided by the stimulation rates of the motor units (a muscle consists of several motor units) and the recruitment of motor units.

The CNS manages coordinated limb motion by controlling in a hierarchical manner. Premotor cortex is responsible for high-level planning of coordinated tasks and instructs the motor cortex to issue the necessary stimuli to the appropriate motor nerves. The motor nerves innervate muscles in an intricate pattern of recruitment so as to produce smooth and dexterous motion. Feedback paths of tactile force, muscle tension, and muscle length allow precise regulation of force output and limb position. See Seeley et al. (2007) for details.

2.2 Electromyography

The study of muscle function through the inquiry of the electrical signal the muscles emanate (Basmajian and DeLuca, 1985).

When a muscle contracts, electrical activity is generated. Electromyography (EMG) is a medical technique for recording and evaluating this extracellular electrical potential.

EMG is performed using an instrument called an electromyograph, to produce a record called an electromyogram. An electromyograph detects the electrical potential generated by muscle cells when these cells contract. Electrodes used in EMG are of a wide variety of type and construction, and their use depends on the principles that they must be relatively harmless for the user/patient, and must be brought close enough to the muscle under study.

There are two main types of electrodes used for the study of muscle behaviour, inserted electrodes and surface electrodes. To perform intramuscular EMG, a needle electrode is inserted through the skin into the muscle tissue. When EMG is used for prosthesis control, the needle electrodes are too painful, and thus surface electrodes are used. The surface electrodes are not as accurate as needle electrodes but are still considered as a good measure of muscle activity or muscle force. These surface electrodes is called myoelectrodes, and the resulting signal is called a surface electromyogram (sEMG). (Muzumdar, 2004a), (Fougner, 2007), (Basmajian and DeLuca, 1985).

2.2.1 Surface electrodes

Surface electrodes can be constructed with an active or passive configuration. In the passive configuration the electrode consists of a detection surface that senses the current on the skin through its skin-electrode interface. In the active configuration, the input impedance of the electrodes is greatly increased, rendering it less sensitive to the impedance of the electrode-skin interface.

The active surface electrodes have been developed to eliminate the need for skin preparation and conducting medium. These are often referred to as dry or pasteless electrodes. These electrodes can be either resistively coupled or capacitively coupled to the skin. In the case of the capacitively coupled electrode, the detection surface is coated with a thin layer of dielectric (nonconducting) substance, and the skin electrode junction behaves as a capacitor. Although the capacitively coupled electrodes have the advantage of not requiring a conductive medium, they have a higher inherent noise level.

The active surface electrodes are preferable not only because they provide an sEMG signal of greater fidelity, but also because they are convenient to use. The simplicity and speed with which they may be applied to the skin is rapidly making them the electrode of choice for pragmatic applications as in myoelectric prosthesis control. The main disadvantages of surface electrodes are that they may be used effectively only with superficial muscles and that they cannot be used to detect signals selectively from small muscles. The detection of cross-talk signals from other adjacent muscles becomes a concern.

2.2.2 Bipolar detection configuration

In the bipolar detection configuration two detection surfaces are used to detect two potentials in the muscle tissue of interest, each with respect to the reference electrode. The two signals are fed to a differential amplifier for elimination of common mode components in the two signals (Figure 2, (Kampas, 2001)).

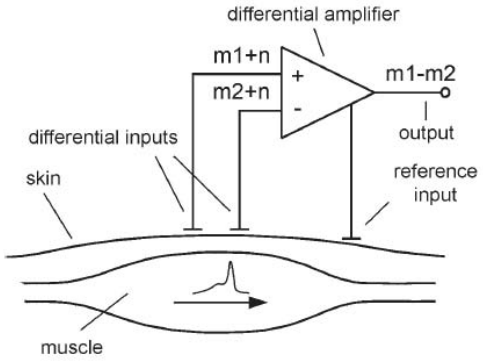

Figure 2: Differential amplifier

The measure of the ability of the differential amplifier to eliminate the common mode signal is called the common mode rejection ratio (CMRR). For an

ideal differential amplifier CMRR = ∞. This idealized behaviour cannot be achieved with present day electronics.

Signals emitting from the muscle tissue of interest near the detection surface will be dissimilar at each detection surface due to the localized electrochemical events occurring in contracting muscle fibers. Whereas AC noise signals originating from a more distant source (such as 50 Hz electromagnetic signals radiating from power cords, outlets and electrical devices) as well as DC noise signals (such as polarization potentials in the metal-electrolyte junction) will be detected with an essentially similar amplitude at both detection surfaces and, therefore, will be subtracted prior to being amplified. The spacing between the signal electrodes also affects the appearance of the sEMG. Wide electrode spacing results in a longer time for the depolarization wave to pass between the two active electrodes, and more smearing of the signal will occur. This again leads to loss of high frequency information in the signal. The smaller the electrode used in prosthesis, the higher frequencies can be detected. A larger interdetection surface spacing will render a lower bandwidth.

2.3 The concept of myoelectric controlled prostheses

This section is cited from Sæther (2007) (some modifications).

2.3.1 The myoelectric signal

The roots of "Myoelectric" involve two words. "Myo", from Greek *mys*, meaning muscle and *electric* referring to electricity. From this, a myoelectric signal (MES) is defined as *the electrical activity produced by a contracting muscle*.

2.3.2 Myoelectric control

The MES (the sEMG after being amplified, rectified and filtered) is an effective and important signal for the control of powered prostheses. Myoelectric control is a broad subject, ranging from the practical aim of providing an amputee with a functional prosthesis to the pursuits of modelling and extracting more and more information from the MES. Conceptually a myoelectric control system can be thought of as a switch that controls the power to an electric terminal device. Surface electrodes on remnant muscles within the residual limb gives a signal that activates the switch. Power comes from a battery that can be recharged. The sEMG in a residual limb is amplified, processed and used to control the flow of electricity from a battery to a motor, which operates an artificial limb (Figure 3).

Voluntarily controlled parameters of MES from a muscle or muscle group are used to select and modulate a function of a multifunction prosthesis. There is also demand for simultaneous movements, that is, the prosthesis should perform more than one function at a time. It is not reasonable to expect that the exquisite control of the CNS should be extracted from the MES, but -hopefully-

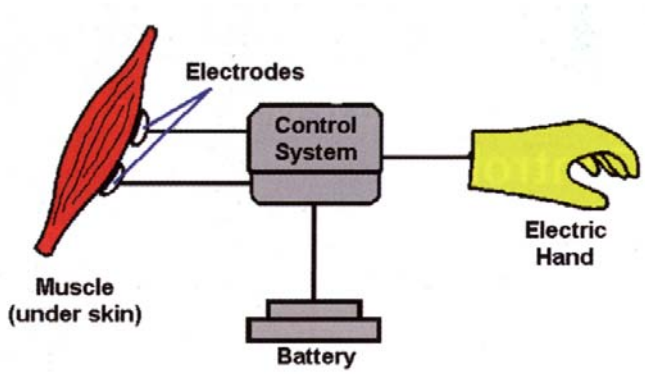

Figure 3: Basic concept of myoelectric control (from Muzumdar (2004a))

with an intelligent control system the prosthesis might be controlled in an acceptable way.

Since myoelectric prostheses control the limbs by converting muscle movements to electrical signals, the amputees are allowed to control the artificial limb more directly. The concept is quite simple, but the design of a clinically useful myoelectric prosthesis is extremely difficult. Challenge of getting a prosthesis that is comfortable to wear increases when the weight of the prosthesis increases.

One of the primary design concerns when using myoelectric control is the power consumption. The system must be battery operated, so the power consumption must be kept to a minimum. All powered prostheses currently on the market employ small rotary DC motors to perform the required movement function.

All myoelectric prostheses need to be adjusted to suit the individual user, both design/interface and control algorithms. An important point in prosthesis control is that the adjustments also go the other way around, the user need to adjust to the prosthesis as well.

2.3.3 Advantages and limitations

Electrically powered prostheses with myoelectric control have several advantages over other types of prostheses:

- The user does not need straps and other harnesses required of body-powered and mechanical switch control prostheses (the prosthesis still has to be fastened to the residual limb, but the prosthesis socket is fitted to the stump)
- The MES is non-invasively detected on the surface of the skin
- The electric battery is possibly the most convenient form of power supply that can be incorporated into a prosthesis

- The controller can be adapted to proportional control with relative ease
- The electronic circuits are continuously improved and miniaturized
- The muscle activity required to provide control signals are relatively small and can resemble the effort required of an intact limb

There are also control limitations in myoelectric control:

- Lack of robustness in the processing of the input (MES) to specify the output (joint-space kinematics) and the disparity of the means of manipulation from natural motor control and learning
- The random nature of the MES and limits on prosthesis activation delay make fine control difficult

(Parker et al. (2004))

For unilateral amputees, the prosthesis is often used mostly as an assistant device. Single-hand movements will usually be done with the healthy hand, not the prosthesis. In this case the prosthesis do not need to perform every possible activity of daily living, it should rather be designed as a supportive device (holding the bread while the healthy hand slices it).

2.3.4 Current research

One thing that is important for prostheses is that they should be a remedy for the amputee, not a burden. The objective in the design of any prosthetic control system must be to allow the amputee to concentrate on things other than the contraction of specific muscles. Control is then done on a subconscious level, this increases the degree of acceptance and efficiency. The goals of current research in myoelectric control is to provide better accuracy in state selection and to present a more natural means of effecting control.

2.4 Artifacts

A structure or feature, visible only as a result of external action or experimental error (Ödman and Öberg (1982)).

Artifacts consists of all types of disturbances in biopotential signals. The motion artifacts in electrode recording are composed of a number of different subcomponents originating from various electrochemical and electrophysiological sequences.

2.4.1 Motion Artifacts

This section is cited from Sæther (2007) with a few modifications.

Surface electromyograms (sEMG) contain artifacts induced by e.g. sweat, motion and external forces. These artifacts are undesirable because they impair the performance of prosthetic control systems.

A well-known problem in myoelectric prostheses is motion artifacts. This is a kind of signal disturbance that arise from movements and varying contact forces between the surface electrode and the skin. The frequency content of motion artifact is typically below 10-20 Hz. The general approach to motion artifact cancellation is to high-pass filter the sEMG with a cutoff frequency of approximately 20 Hz. Little "true" signal power is lost, however some motion artifacts is rejected. But not always all of the artifacts. These artifacts can cause unwanted behaviour of the prosthesis.

There are at least two sources of motion artifact in surface electrodes: mechanical disturbance of the electrode charge layer and deformation of the skin under the electrodes.

The first type occurs when there is relative movement between the electrode and the underlying skin. If this happens a noise signal is produced. This signal is similar to the sEMG and can be confused with the true sEMG. In severe cases this motion artifact looks like a contraction to the control system. Figure 4

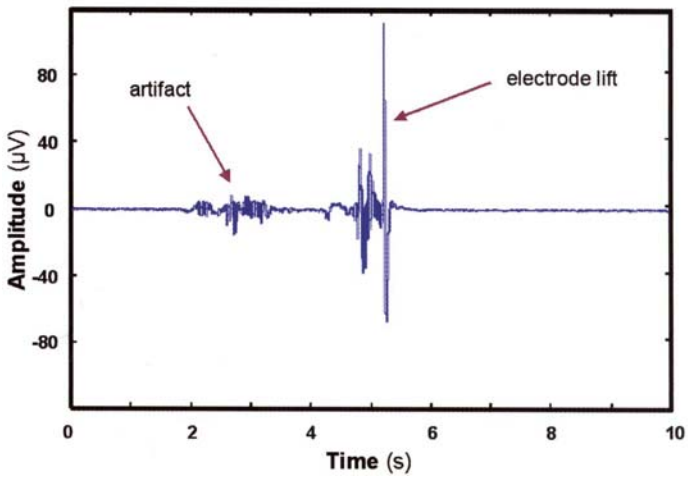

Figure 4: Motion artifact & electrode lift (from Muzumdar (2004a))

shows the phenomenon where a surface electrode has been moved sideways. A surface electrode converts the ionic activity of a contracting muscle into an electric current, just like a transducer. This process sets up a charge double layer at the electrode-skin interface, which can be mechanically disturbed. This situation is analogous to that of a parallel plate capacitor in which the separation of the plates and the area are variable. When using this simple model and the charge at the interface is assumed constant, then the artifact developed is dependent on the relative movement of the electrode with respect to the electrolyte/skin. The magnitude of this artifact component is highly dependent on the nature of the electrode material.

Skin stretch reflex is a second phenomena leading to motion artifacts. These motion artifacts arise because a potential difference, the skin potential, exists

across the layers of the epidermis (upper layers of the skin), and the value of this potential changes when the skin is stretched or deformed. This component of motion artifacts is independent of electrode material. In short-term laboratory studies, this type of artifacts can be minimised by reducing the skin impedance by removing the upper layers of the skin by abrasion (Tam and Webster, 1977), and the use of electrode gels that are rich in ions. In myoelectric control when the prosthesis is used on a long-term basis, this is not favourable, and is of limited use.

An approach in this situation, is to avoid relative movement between the myoelectrode and the skin surface. This demands a very good fitting between the socket and the residual limb. When the prosthesis is exposed to an external load, this fitting should be such that there should be no relative movement between the myoelectrodes in the prosthesis and the residual limb. An extreme case is if the myoelectrode completely loses contact with the skin. This is called electrode lift, and an example is showed in Figure 4. When an electrode lift occurs, the result is often uncontrolled and unsolicited prosthesis behaviour. This is because the common-mode voltage of the body is present on one electrode and not the other. The differential amplifier fails to remove the domestic supply voltage interference and the prosthesis is effectively driven by the 50 Hz interference rather than the MES. (Muzumdar, 2004b).

Another approach is considered in this thesis, namely using force sensing sensors to cancel motion artifacts.

Motion artifact can be reduced in sEMG recordings through signal conditioning. Conforto et al. have compared four techniques for motion artifact removal from sEMG:
- Filtering with an eight order Chebyshev high pass filter with corner frequency at 20 Hz,
- Filtering with a moving average filter to estimate the motion artifact and subtracting the estimated artifact from the signal record,
- Filtering with a moving median filter to estimate the motion artifact and subtracting the estimated artifact from the signal record,
- Filtering using an adaptive filter based on orthogonal Meyer Wavelets (See Clancy, Morin, and Merletti (2002) for more).

Luca et al. (2006) have tested the electro-mechanical performance of different active sEMG sensors. Their findings shows that contouring the electrode surface using a more aggressive double-sided tape increases the adhesive performance of sensors compared to more standard configurations. Application of a hydro gel to the sensor contacts should be used with caution to avoid motion artifacts resulting from mechanical perturbations. Their work showed that the use of a surfactant did not provide obvious advantages over through skin preparation when assessing perturbations.

2.4.2 Other types of artifacts

Electrical artifacts produced by the heart may contaminate EMG signals when recording surface EMG from torso muscles. This source of noise is a problem for myoelectric prosthesis control in a patient with bilateral amputations at shoulder disarticulation level, where the control signals are taken from the reinnervated pectoralis muscles of the patient. Zhou, Lowery, ff Weir, and Kuiken (2005) have looked on removal of ECG (electrocardiogram) artifacts from myoelectric prosthesis control signals developed by targeted muscle reinnervation. See also (Zhou et al., 2007).

Risdal (2006) have considered the possibility of adaptive filtering for compression artifact removal. He takes use of the MultiChannel Recursive Adaptive Matching Pursuit (MC-RAMP). See Appendix A in his PhD Thesis.

To obtain readable recordings of electrophysiological events through surface electrodes, the skin impedance between recording electrodes must be kept low. Various methods have been tried for reducing skin impedance enough to obtain recordings with little noise but without unduly hurting the subject. Okamoto et al. (1987) introduced a method of lightly scratching the skin with a needle. This dramatically lowers the skin impedance and is relatively painless. This method is not practical in prosthetic issues.

2.4.3 Motion artifact removal methods used in ECG (electrocardiogram)

The reason for including this section is that possibly, some of these methods can be used in artifact removal in myoelectric prosthesis control as well as in ECG.

Motion artifact can produce large amplitude signals in the ECG that may be misinterpreted by clinicians and automated systems resulting in misdiagnosis, prolonged procedure duration and delayed/inappropriate treatment decisions.

Hamilton and Curley (1997) have demonstrated that adaptive filtering significantly can reduce motion artifact in ECG recordings, using a signal that is related to skin stretch. Skin potentials from the forearm were measured with three Ag-AgCl electrodes and a standard ECG amplifier. At the same time the skin stretch was measured with a miniature displacement sensor. The skin stretch signal from the sensor on the electrode was filtered with a digital filter whose coefficients were calculated adaptively using an LMS (least mean square) algorithm with signal statistics calculated from the entire data set. The filtered signal from the sensor was then subtracted from the skin potential signal. The motion artifacts were manually generated by pulling on the skin on either side of the electrode and by pushing directly on the center of the electrode. In a practical system, two sensors should be required for each electrode. The sensors used in this test were very expensive. The ideal system would require a sensor sufficiently inexpensive that it could be incorporated into a disposable electrode.

Like Hamilton and Curley (1997), Tong et al. (2002) have investigated the possibility of adaptive reduction of motion artifact in the ECG. Their hypothesis: motion artifact can be reduced using electrode motion as a reference signal to an adaptive filter. Their conclusion were that using electrode motion as measured by either an anisotropic magnetoresistive sensor or accelerometers as the input to an adaptive filter reduces the amount of motion artifact present in the ECG.

Liu and Pecht (2006) have developed a method/hardware to directly measure skin stretch simultaneously with the ECG. An optical sensor is used to capture the skin strain, this sensor is integrated in an ECG electrode. Using this skin stretch data, skin stretch induced noise will be reduced in the measured ECG with adaptive filtering technique.

3 Aim of the study

Surface electromyograms (sEMG) contain artifacts induced by e.g. sweat, motion and external forces. A well-known problem in myoelectric prosthesis control is the presence of motion artifacts. These are signal variations caused by relative motion and varying contact forces at the surface electrode-skin interface (electrode-electrolyte junction). These artifacts are undesirable because they impair the performance of the prosthesis control systems, and are known to cause unsolicited prosthesis behaviour. Despite these problems, comparative studies of artifact cancellation techniques in myoelectric prosthesis control are extremely limited in the research literature.

The main purpose of this study is to consider the effect motion artifacts have on myoelectric prosthesis control (the problem with sweat is disregarded). To control myoelectric prostheses in a proper manner, it is significant to minimise the effect of these motion artifacts.

A prototype sEMG sensor with built-in force sensing resistors (FSRs) (developed in Sæther (2007)), will be improved, characterized and used to measure external forces the sensor is exposed for. Potentially the artifacts caused by these forces can be cancelled by taking the signals from the FSRs into consideration when estimating muscle force. The long term goals are to contribute to advanced sEMG sensor design and set guidelines for their use.

Hypothesis: Cancel the effect motion artifacts have on sEMG-based contraction estimate.

4 Laboratory Equipment

In this section the equipment at the EMG/FES laboratory of the Department of Engineering Cybernetics will be presented. This section is cited from Sæther (2007) with a few modifications.

4.1 Equipment on the laboratory

- Digitimer Ltd NL844 Pre-Amplifier
- NeuroLog by Digitimer, model NL900D
- BNC-2090, National Instruments
- PCI6251, DAQ-card

4.1.1 sEMG sampling equipment

The NL844 is a four channel pre-amplifier with input impedance 100MΩ. Its low noise and high impedance differential inputs make it particularly suitable for use as a headstage pre-amplifier. It is ideal for isolated EMG, electroencephalography (EEG) or electrocardiogram (ECG) applications. This pre-amplifier has a fast recovery time from stimulus artifact pulses.

The pre-amplifier is connected to an isolator (NL820) (inside the NL900D). This isolator is internally coupled to a filter, NL135. The output from the filter is coupled to a BNC input on an adapter, BNC-2090. The adapter is again coupled to a DAQ-card from National Instruments, PCI6251. See Figure 5.

The DAQ-card processes the sEMG, and imports it to Matlab (and Simulink). An S-function is responsible for this transmission. The S-function is the driver of the DAQ-card, and it is implemented in C. The source code is available for use at the EMG/FES laboratory (and also in Appendix E). Matlab has a limited sampling frequency, maximum 100 Hz. This is too slow for the MES, which lies in the area 0-500 Hz. The DAQ-card resolves this problem by sampling the signals into a buffer, Matlab empties this buffer for each sample. (Midtgaard, 2006).
(Information in this section is fetched from NationalInstruments (2008) and Digitimer (2008))

Figure 5: Signal processing equipment. Myoelectrode - NL844 - NL900D - BNC-2090 - PCI6251 (from top to bottom)

4.1.2 Force- and sEMG sampling equipment

A sensor for collection of sEMG and external forces (causing motion artifacts) has been constructed, see section 6. An analogue load cell (Waegezelle Z6FC3 from Hottinger Baldwin Messtechnik) for recording muscle force contraction from a test subject is also used (Figure 6).

Figure 6: Load cell (from HBM (2008))

4.1.3 Connections and earthings

Figure 7 shows a circuit diagram of all the connections and earthings on the laboratory.

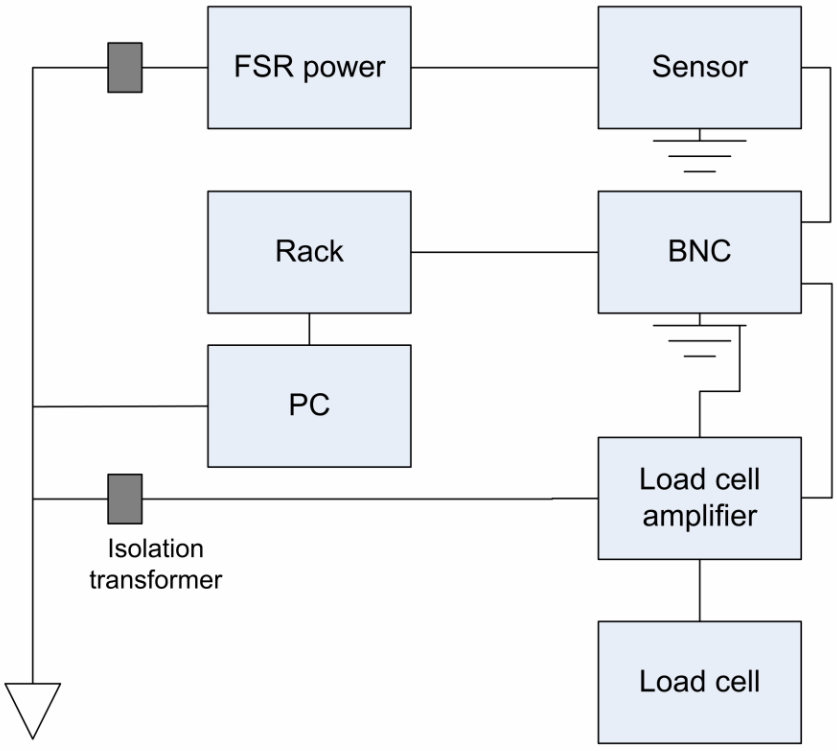

Figure 7: Laboratory connections

5 Model of the surface electrode - skin junction

When modelling the surface electrode-skin junction, several factors have to be considered. In this section some of these factors are discussed.

5.1 Impedance

All forms of matter (also tissue and skin) present an impedance to the transmission of an electric current. The impedance function is a vector quantity, hence it is expressed in terms of complex numbers. The real part denotes the resistance and the imaginary part denotes the susceptance.

Tissue resistance depends on tissue type and tissue orientation. Body resistance is not a fixed quantity, it varies from person to person from time to time (www.allaboutcircuits.com (2008)). The farther the EMG signal needs to travel through body tissue before reaching the surface electrodes, the more resistance it encounters. Energy is absorbed by the resistance, and the result is that less of the original energy reaches the surface electrode. Body tissues tend to absorb higher-frequency components of the signal, allowing lower frequencies to pass through more readily (body tissue works as a low pass filter).

If there is adipose tissue between the muscle and the surface electrodes, more of the signal gets absorbed. A fatty layer acts like an imperfect electrical insulator between the muscle and the electrodes. The fatty layer plays a larger role in the interpretation of resting sEMG values (isometric contractions) than in dynamic sEMG recordings.

The latter part of the impedance function (susceptance) exists due to the presence of capacitance and/or inductance, two basic electrical properties of matter. In media such as muscle tissue, fatty tissue, and skin, the inductance is essentially immeasurable. However, the capacitance is present in a significant amount and cannot be ignored. The impedance between the surface electrode and the skin is a delicate matter, and it is important to keep the impedance of the skin at the electrode site as low as possible.

5.2 The surface electrode-skin junction

The sEMG sensor is an electrochemical transducer that detects biopotentials using metallic contacts placed on the skin tissue. One of the simplest expressions of an impedance function, which is useful for conceptualising the electrical characteristics of electrodes and tissue, is the impedance of a resistance in series with a capacitor, see Figure 8. Here, only one of the surface electrodes is modelled (in bipolar detection two surface electrodes are used), but the same situation are applicable for the other electrode as well. A surface electrode works as a power converter. It converts ionic activity from a contracting muscle to an electric current. This process allows accumulation of electric energy between the surface electrode and the skin. This can be disturbed mechanical, as described in section 2, and appears as motion artifacts. A similar situation

occurs in a plate capacitor. Separation of the plates and the area varies. In this

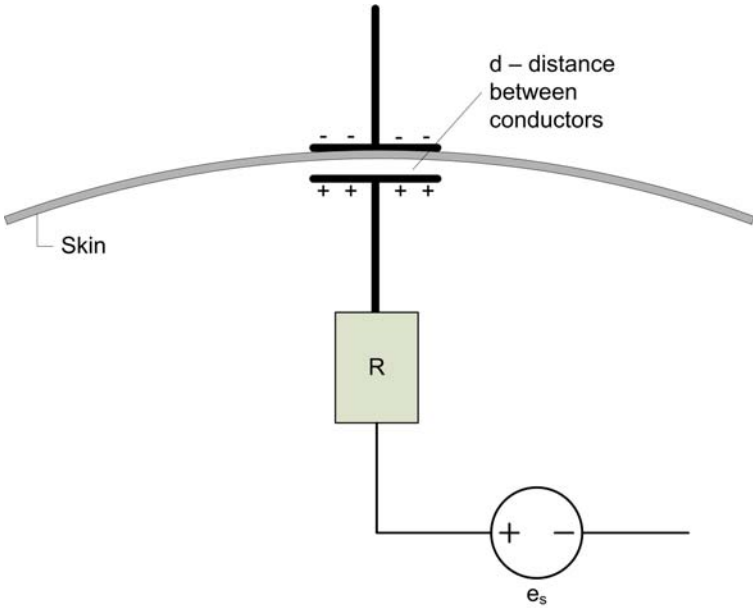

Figure 8: Model of the surface electrode - skin junction

configuration the impedance function is expressed as a vector $Z(\omega)$:

$$Z(\omega) = R + \frac{1}{j\omega C} \tag{1}$$

R - Resistance (Ω - Ohm), C - Capacitance (F - Farad)

The capacitance increases when pushing the electrode closer to the skin (common area of the conductors (A) increases - distance (d) decreases) $\Rightarrow$ the voltage decreases and the amplitude is affected. From this it follows that the equation of the capacitance should be a function of area and distance, as in equation 2.

$$C = f(A, d) = \varepsilon_0 \cdot \varepsilon \cdot \frac{A}{d} \tag{2}$$

- ε_0 - Permittivity, vacuum = 8.8542 * 10e-12 F/m
- ε - Relative permittivity of the matter
- A - Conductor area
- d - Distance between the conductors

Equation 3 is a suggestion of a linear model of how the area changes. Taking the last part into consideration makes it a Taylor model. The reason for including a non-linear part in the equation can be to keep the effect when a lopsided

pressure is applied. A_0 is the initial area, and F is the external force applied (causing motion artifacts).

$$A = A_0 + A_1F(+A_2F^2 + \cdots) \tag{3}$$

Equation 4 is a model of how the distance between the conductors changes. d_0 is the initial distance, and F is the external force applied.

$$d = d_0 - d_1F \tag{4}$$

The resulting sEMG signal becomes

$$sEMG = f(e_s) + g(F) \tag{5}$$

F in equation 5 should be derived from equations 3 and 4.

5.2.1 Input impedance and Input bias current

The importance of the CMRR (see section 2) becomes apparent when dealing with the effects of external fields such as power-line induced interference radiating from the environment.

The effect of an external signal field acting on the tissue media can be modelled as in Figure 9. Two current sources (i_n) in parallel with their respective tissue impedances (z_{tn}). If the tissue media impedance (z_n) is isotropic, and the external field gradient across the tissue media is constant, the fields induced currents (i_n) at each input are equal and will cancel. The higher the CMRR of the amplifier, the better cancellation of these undesirable currents.

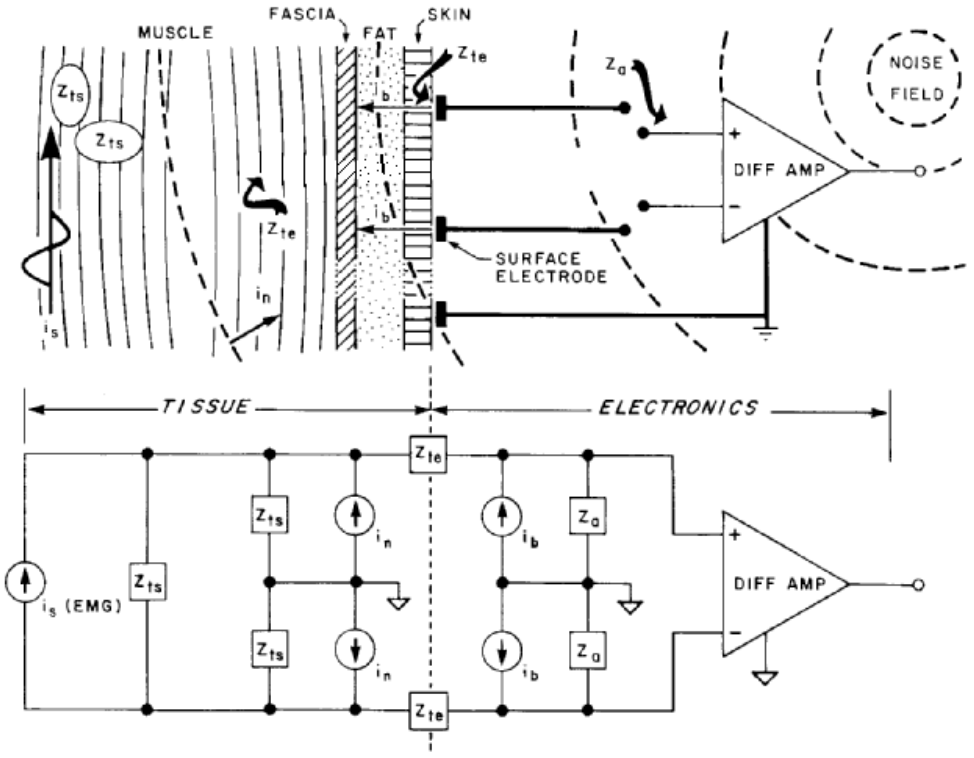

Figure 9: Upper part of figure: Diagram representation of impedances and currents in the tissues, electrode and amplifier, lower part: Circuit diagram, representing the electrical interaction of the EMG signal, external noise, electrode and amplifier (From Basmajian and DeLuca (1985))

i_s - source current from EMG signal

z_{ts} - tissue impedance seen by source current

z_{tn} - tissue impedance seen by noise current

i_n - common current for noise

z_{te} - tissue electrode impedance of the metal electrolyte interface

i_b - input bias current from amplifier

z_a - input impedance of amplifier (100 MΩ)

z_{te} and currents are varying with pressure.

In order to measure the sEMG signal in an accurate way, it is necessary to understand how the input impedance and input bias current of the differential amplifier can influence the amplitude and shape of the sEMG.

Input bias current can be thought of as the minimal constant current required keeping the differential amplifier active. The differential amplifier has a

finite impedance at each input, and nonzero input bias current. The bias current flows out of the amplifier (demonstrated in Figure 9), this leads to no amplification of any signal which has a current less than the bias current. This is not a problem when using surface electrodes.

The distributed impedance of the sEMG signal source is determined by the impedance characteristics of the tissue (z_{ts}) and the tissue-electrode interface (z_{te}). These impedances have resistive and reactive components due to the capacitive effects of tissue media and electrode interface. Distributed source impedance can vary greatly, depending on the impedance of the surface electrode interface configuration (z_{te}) and amount of intervening tissue (z_{ts}) (Basmajian and DeLuca, 1985).

To minimise wave shape distortion and attenuation of the signal source (muscle) due to the shunting by the amplifier, the input impedance (z_a) should be much larger than the distributed source impedance. The input impedance of the amplifier used in this experiment is 100 MΩ. The input impedance of the sEMG preamplifier should be 10 to 100 times greater than the impedance at the electrode-skin interface. High input impedance of the sEMG preamplifier makes the sEMG more robust to poor electrode-skin connections.

6 The prototype sEMG sensor

6.1 Construction of the sensor

It has been developed a prototype sEMG sensor with three built-in force sensing resistors (FSRs). This sensor is used for recording sEMG and contact forces between surface electrode and skin (applied to the sensor as external forces). The sensor consists of two parts, a surface electrode and an FSR array.

6.1.1 Construction of the surface electrode

The surface electrode unit was built from the metal parts of an Otto Bock 13E125 electrode, mounted with the original spacing (on a plastic plate) and then wired to an external preamplifier.

The reference electrode is positioned in between the two signal electrodes, and has a larger surface area than the signal electrodes. This large surface area will lower the impedance of the reference electrode and helps to reduce the line-bourne interference due to a reduction of the common mode voltage on the body (Muzumdar (2004a)). The surface electrode unit is showed in Figure 10.

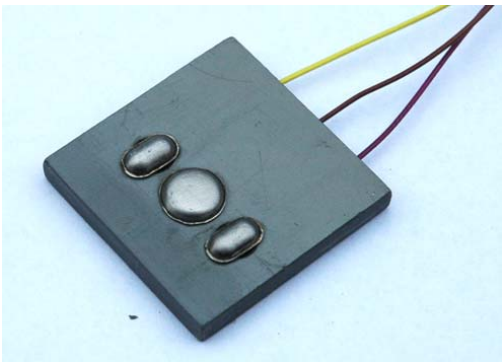

Figure 10: Surface electrode

6.1.2 Construction of equipment for recording force/pressure changes

To measure the contact forces between the surface electrode and the skin, a proper sensor type had to be chosen. The final choice landed on force sensing resistors (FSRs). FSRs were chosen as force sensors due to their flatness and simplicity of use. A model that was readily available was used (Quadratic FSRs (2.7cm · 2.8cm) made by the company Interlink Electronics). With a more appropriate size and shape, the entire device easily fits into a prosthesis socket.

An FSR use the electrical property of resistance to measure the force (or pressure) applied to a sensor. An FSR is made up of two parts (three with the plastic spacer). The first is a resistive material applied to a film. The second part is a set of digitating contacts applied to another film (the active area). The

different parts of an FSR are showed in Figure 11.

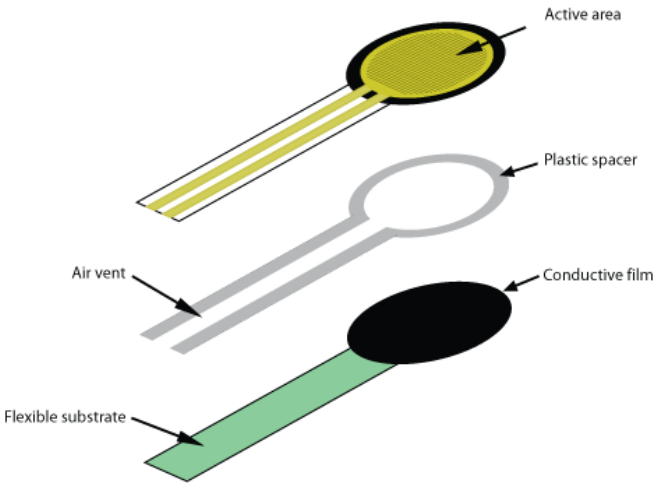

Figure 11: Force sensing resistor (SensorWiki (2008))

When an external force is applied to the sensor, the resistive element is deformed against the substrate. Air from the spacer opening is pushed through the air vent in the tail, and the conductive material on the substrate comes into contact with parts of the active area. The more of the active area that touches the conductive element, the lower the resistance. The resistance of an FSR is inversely proportional to the force applied.

General FSR characteristics:

- The appearance of an FSR is a great advantage. With an appropriate size and shape, the sensor fits into a prosthesis socket. Size range: 0.5 cm$\times$0.5 cm to 51 cm$\times$61 cm. Thickness range: 0.20 mm to 1.25 mm.
- The signal from an FSR does not need pre-amplifying
- Insensitive to noise and electromagnetic fields
- Chemical, moisture and temperature resistant (temperature range: -30°C to 70°C)
- Force Sensitivity Range: $<$ 100 g to $>$ 10 kg
- Contain no moving parts and are robust under repetitive use (lifetime $>$ 10 million actuations)
- Responsive to variations in applied pressure
- Operates at much lower currents and cost in comparison to similar sensing devices

(Information from InterlinkElectronics (2008))

An important property with FSRs is that they are notoriously non-linear in response to pressure. Signals from the FSRs are easily processed in Matlab/Simulink together with the sEMG.

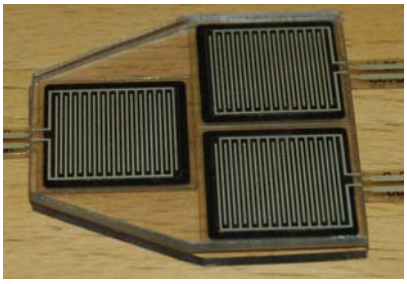

Figure 12: FSR array

The sensors were sandwiched between two layers of plexiglass using double sided tape (Figure 12). The electrodes were attached to this structure with the reference electrode at the center of the FSR array.
With particular designs of FSRs it is possible not only to measure the force but also the position of that force (good spatial resolution). The reason for using three FSRs, and this placement of the FSRs, is to try to capture the x-position, y-position and the size of the pressure forces.

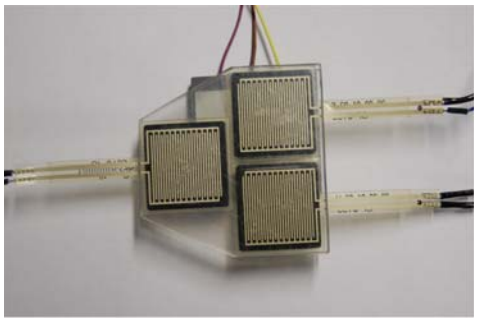

13a: Top side, external forces applied to this side

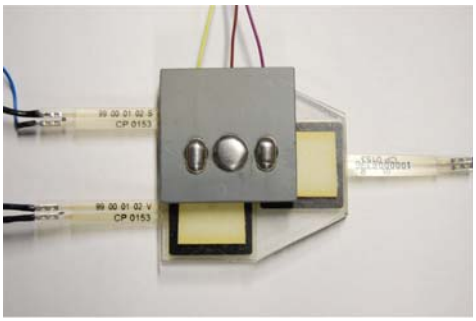

13b: Underside

The prototype sensor is showed in Figures 13a and 13b. Figure 13c shows the sensor structure schematic, and the actual sensor structure in Figure 13d. From top to bottom: Plexiglas - FSRs - mounting tape - plexiglas - mounting tape - plastic plate - surface electrodes.

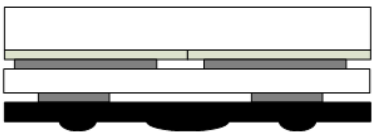

13c: Sensor structure (schematic)

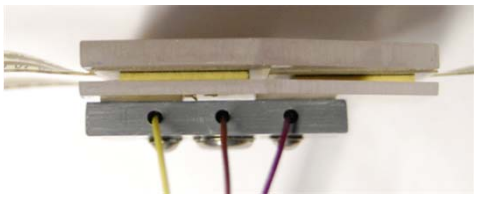

13d: Sensor structure

Three similar circuits (voltage dividers) are used for collection of force or pressure changes on the FSRs. The circuit diagram is showed in Figure 14. R_{FSR} is the resistance of the FSR, R_{Pot} is the resistance of a potentiometer (potmeter). The potmeter needs to have a high resistance to minimise the current through the FSR to prevent damage to the sensor.

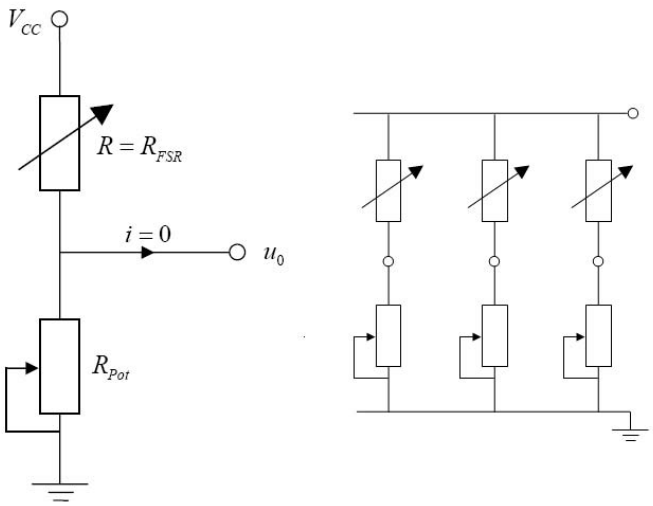

Figure 14: Circuit diagram

The equation of the voltage divider is computed in Sæther (2007), and given in Equation 6.

$$R_{FSR} = R_{Pot}(\frac{V_{cc}}{u_0} - 1) \tag{6}$$

u_0 is the measured voltage, everything else is known.
Choice of potmeter values is also described in Sæther (2007). The potmeters used in the circuit can be varied between 0 and 500kΩ. Used resistance: 368kΩ.

The circuits are connected by BNC-connectors to the BNC-adapter, in this way the signals (u_0) are imported to Simulink together with the sEMG. The Simulink diagram used is showed in Appendix B.

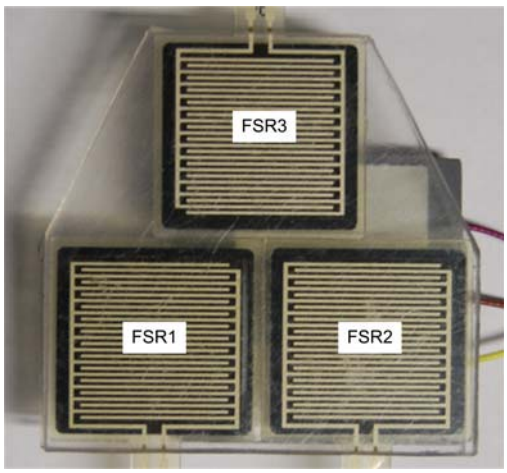

Figure 15: Placement of the three FSRs

6.2 Improvements of the sensor

Because the FSR's operation is dependent on its deformation, it works best when affixed to a support that is firm, flat, and smooth. An FSR have a raised part around the outer edge, in Sæther (2007) the applied pressure had to be heavy to get an excursion at all. The three FSRs were sandwiched between to layers of plexiglass, and the reason for this non-sensitiveness is this raised part. To get in touch with the sensing area, the plexiglass practically had to be bent. This problem was solved by mounting the sensors to the plexiglass with a strong double-sided mounting tape from Scotch, thickness 2 mm. This mounting tape was placed on the active area, avoiding the raised part of the sensors.

A problem that emerged under data acquisition, was that the signals from the FSRs and the load cell brought into the rack were influencing each other. After testing all the equipment, wires and earthing connections, the problem occurred to be in the rack with the BNC-plugs. To cancel this effect, terminators were attached to each BNC-plug. A terminator is a component that closes a circuit and allows the current to pass through this circuit. The resulting signals got weaker, but are still in due proportion to each other (no need for amplification).

7 Method description

7.1 Characterization of the prototype sEMG sensor

The purpose with this characterization is to see the effect of pressure applied on various locations on the sensor to get a compounded sensor that can "feel"/measure applied pressure on a larger surface.

7.1.1 Characterization set-up

The FSR signals and the load cell are all imported into Matlab (and Simulink), therefore the load cell was used in the characterization. The load cell gives a more accurate measure of the applied force, instead of using a hand-held dynamometer. An aluminium plate (thickness 3mm) was affixed to the load cell as an extension, see Figure 16. The sensor was placed at the end of the extension, mounted with Scotch tape. This is showed in Figure 17.

Figure 16: Load cell extension

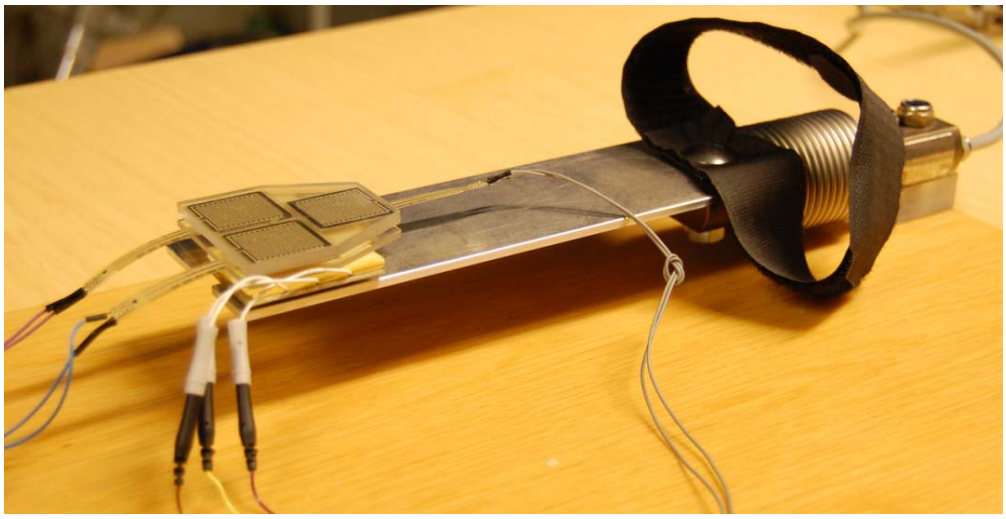

Figure 17: Sensor and load cell

7.1.2 Characterization points

Nine points were selected for characterization. The center of each FSR and some points (two or three) the FSRs had in common should be tested. The sensor was placed in a coordinate system, and points chosen are showed in Table 1. Instead of using the coordinates of the points, the grid in the right part of Figure 18 is used for characterization (for simplicity).

X	Y	Category	Point in grid
1.4	1.35	+	11
4.2	1.35	+	13
2.8	4.05	+	32
1.4	2.7	○	21
2.8	2.7	○	22
4.2	2.7	○	23
2.8	1.35	○	12
1.4	4.05	x	31
4.2	4.05	x	33

Table 1: Points for characterization

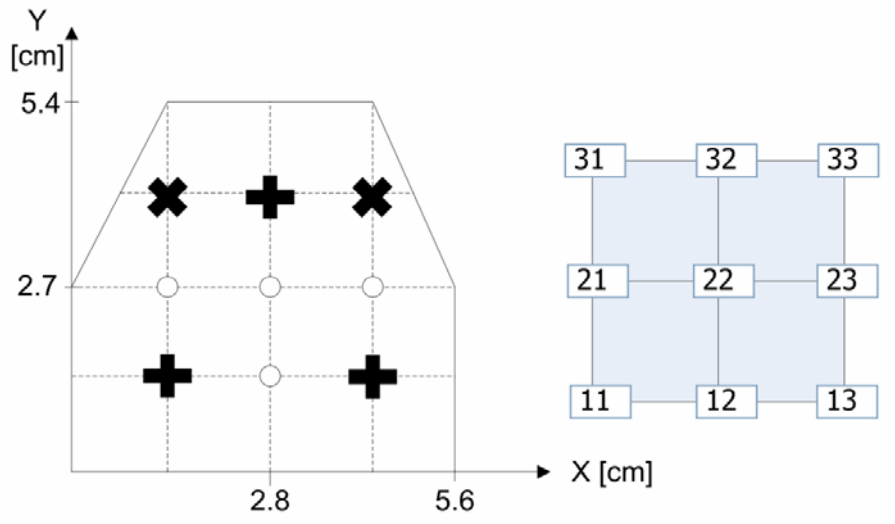

Figure 18: Grid for characterization. Left: category, right: point in grid (see Table 1)

7.2 Experiment protocol

This section is further developed from the experiment protocol in Sæther (2007).

The test subject is a male, 26 years old, athletic, regularly exercising.
The sensor should be tested by simultaneously measuring sEMG (F_{sEMG}) on m. biceps brachii (right arm), FSR outputs (F_{FSR}) and muscle contraction force (F_{muscle}) using an analogue load cell. External forces ($F_{external}$) are deliberately applied to the sensor to affect the sEMG measurements.

The arm can be divided into anterior and posterior compartments. Biceps brachii and brachialis occupies mostly of the anterior compartment. These muscles are the primary flexors of the elbow. The brachioradialis (actually a posterior forearm muscle) helps flex the elbow. See Figure 19. The upper arm's two

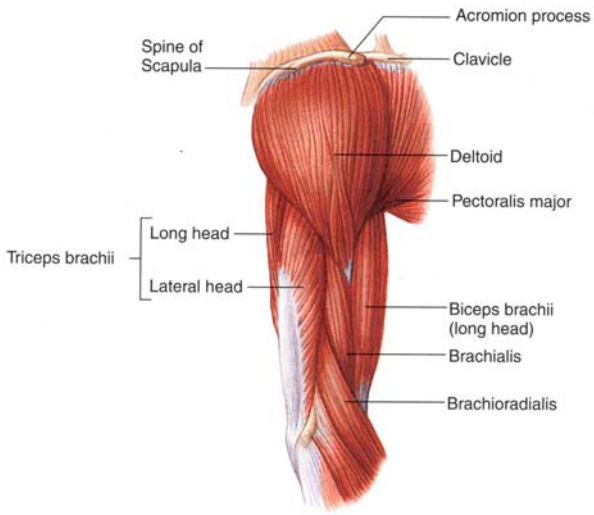

Figure 19: Arm muscles (from Seeley et al. (2007))

headed flexor, biceps brachii, is chosen as measuring point for convenience. The contribution from the brachioradialis muscle to the flexion force has been shown to be small when the hand is situated in fully supinated position. It is assumed that the contribution from all muscles including the antagonist triceps brachii, aside from the biceps brachii could be neglected.

The test subject is seated upright in a chair and positioned in a standarised fashion. The upper arm of the test subject should be hold vertical, the elbow firmly supported on a wooden board with the affixed load cell (a piece of foam rubber between the elbow and the wooden board). The forearm should be horizontal, such that the elbow is sustained in a 90 degree angle. The hand is fully supinated but relaxed. This posture is reported to minimize the contributions of synergetic muscles to the elbow flexion torque. The load cell is applied by means of a strap enclosing the wrist of the test subject. This strap is placed just above the tendon of flexor carpi radialis and flexor carpi ulnaris. See Figure 20.

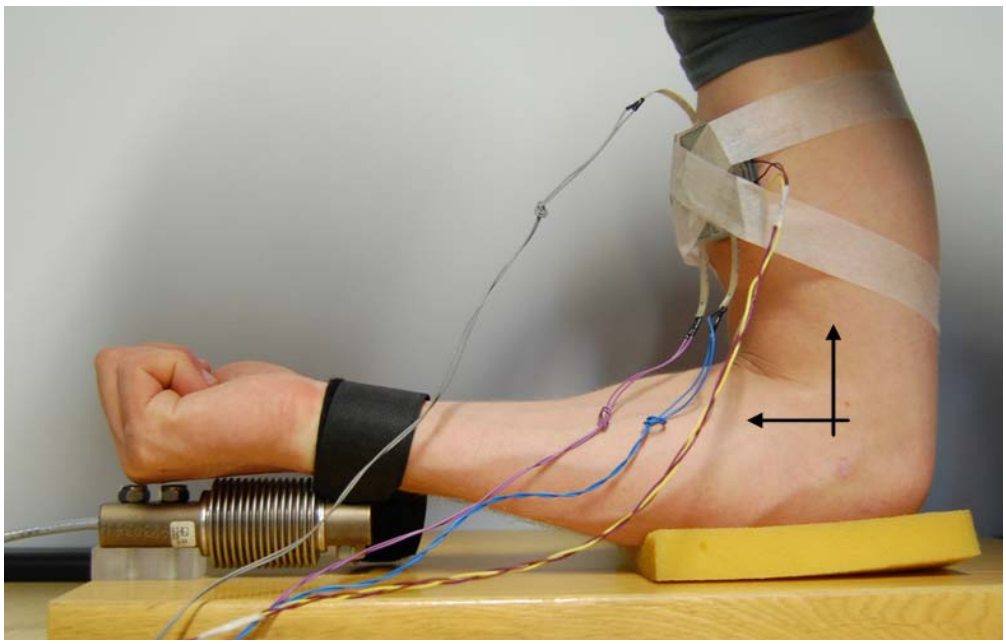

Figure 20: Experimental setup

The detection electrodes (for sEMG recordings) are applied (by adhesive tape) proximal to the innervation zone of the medial head of the biceps brachii muscle. The most distal electrode is applied at ∼45% of the total length of the muscle from the proximal end of the muscle. The sensor is attached to the arm by adhesive tape. It is important to attach the sensor in such a way that the surface electrode is above the muscle when contracting (the muscle moves under contraction).

The external force, $F_{external}$, is applied at the center of the sensor by means of the blunt end of a pen. The range of this force should be from zero external force applied to a maximum $F_{external}$, this maximum external force depends on the saturation of the FSRs and how much force the test subject can stand without feeling pain.

Muscle force/contraction force should be varied in a dynamic/gradually manner. External forces should also be applied when the test subject is relaxing. Target curves for the different forces are showed in Figure 21. The upper part of the figure shows target levels for the contraction force (for the test subject), and the lower part shows target levels for the external force (applied by the author).

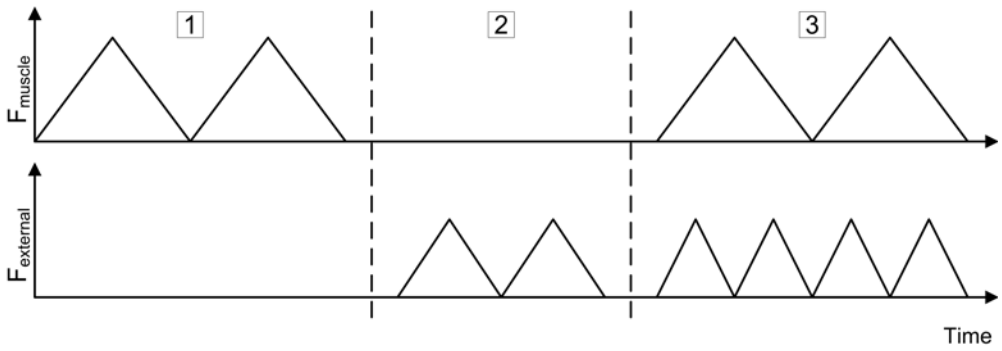

Figure 21: Target curves

1. Test subject is contracting (and relaxing) the muscle without external forces applied, only F_{muscle}

2. Only external forces, $F_{external}$, are applied to the sensor when test subject is relaxing (creating motion artifacts)

3. Both F_{muscle} and $F_{external}$

For each test, three different data sets are recorded. Set 1 (training set) and set 2 (validation set) are recorded with the sensor attached to the same spot with the same adhesive tape. Set 3 (testing set) is recorded after having removed and then reapplied the sensor to the test subject's arm.

This experiment protocol is inspired by Philipson and Larsson (1987); Øyvind Stavdahl et al. (1997)

7.3 Muscle force estimation

This section is cited from Fougner (2007), but adjusted to force estimation (instead of angle estimates). The goal is to estimate muscle force based on the MES and FSR signals, using pattern recognition methods.

7.3.1 Problem description

The load cell is essential when calculating input data for the pattern recognition methods. The load cell gives series of reference values F_j, representing the contraction force from the test subjects arm on which sEMG signals are measured. Measured F_j are the ideal values, while the pattern recognition methods calculates estimates $\hat{F}_j$. The final goal with these methods will be to minimise the error $e_j = (F_j - \hat{F}_j)$. This process will be performed on a training data set, and then the calculated function parameters/relations may be used to find estimated muscle force $\hat{F}_j$. Minimising of the error can be done in several ways, but the conventional method is used in this study: least-squares estimation.

7.3.2 Linear mapping function

$$f_j(X) = W_j^T X + \omega_{0j} \tag{7}$$

The linear mapping function is given in equation 7 (Midtgaard (2006)).

$$f_j(X) = X \rightarrow \hat{F}_j \mid \min_{\hat{F}_j}(F_j - \hat{F}_j)^2 \tag{8}$$

$$\hat{F}_j = g(f_j(X)) \tag{9}$$

Least-squares estimation (equation 8) is used to find the best values of W_j and ω_{0j}. This is done with the Matlab function `FirstOrderEstimation.m` in Appendix A.2 (Fougner (2007)). `FirstOrderEstimation.m` returns the values $\hat{F}_j$.

7.3.3 Quadratic mapping function

An alternative is the quadratic mapping function.

$$f_j(X) = X^T W_{1j} X + W_{2j}^T X + \omega_{0j} \tag{10}$$

Since X consists of measured sEMG signal and FSR signals, the rest of the minimizing to find the best values of W_{1j}, W_{2j} and ω_{0j} is analog to the linear case. This is done with the Matlab function `SecondOrderEstimation.m` in Appendix A.3 (Fougner (2007)). `SecondOrderEstimation.m` returnes the values $\hat{F}_j$.

7.3.4 Multi-layer perceptron network

This section is based on Enderle et al. (2006).

A Multi-layer perceptron (MLP) network is a special version of an Artificial Neural Network (ANN) and is a pattern recognition method commonly used on bioelectric signals. It can be constructed by built-in functions of the Neural Network Toolbox in Matlab. A simple MLP network consists of three layers of nodes (also called neurons) and is a simplified model of how the network in a human brain works. The first layer is called input layer and has as many nodes as input signals. The middle layer is called hidden layer and most of the processing occurs in this layer. The size of this layer is important for the result of the estimation. The third layer, output layer, defines the output signals. Each node in the MLP network does a summation of all the inputs and a bias value, and a transfer function to generate the output. In the Neural Network Toolbox, a useful transfer function is tansig (Hyperbolic tangent sigmoid transfer function, equation 11). It is mathematically equivalent to tanh, with some numerical differences, but it is faster to calculate.

$$tansig(x) = \frac{2}{(1 + e^{-2x}) - 1} \tag{11}$$

The MLP network in this project is trained using least-squares estimation and back-propagation. In this process, the derivative of the transfer function is used,

and that is the reason why a smooth transfer function is chosen. The derivative of the tansig function is a very simple calculation and makes the training process fast. When the MLP network is made with tansig transfer functions in every node, and the number of nodes is equal to the number of parameters in one of the mapping functions, the MLP network and the mapping function actually gives the same result.

The MLP network may be a good alternative to the mapping functions. Of the three methods mentioned, the MLP network can be implemented faster and is also easier to improve or extend, by adjusting a few parameters, but it is trained slower than the mapping functions. Since the training is done offline, not in real time inside a prosthesis, the training time is not that important and the MLP network may be useful.

The MLP network is implemented in the Matlab function `neuralNetwork.m` in Appendix A.4 (Fougner (2007)).

7.4 sEMG filtering procedure

To make a smooth representation of the sEMG's amplitude, a filtering procedure are carried through. This is described in section 5.3.1 in Fougner (2007).

8 Findings/Results

In this section, plots[1] and observations are presented. General discussion of the results in section 9.

8.1 Characterization of the prototype sEMG sensor

8.1.1 Characterization plots

External forces were applied to the sensor when attached to the load cell. A hand-held dynamometer was used, and force was applied in a dynamic manner from zero to one kg, and then back again to zero external force. This was done for each of the nine characterization points.

Figure 22 shows the relationship between FSRs and pressure applied to the sensors (recordings from May 19, 2008). FSR values are plotted as functions of the output from the load cell. (See Figure 15 in section 6 for placement of the three sensors.)

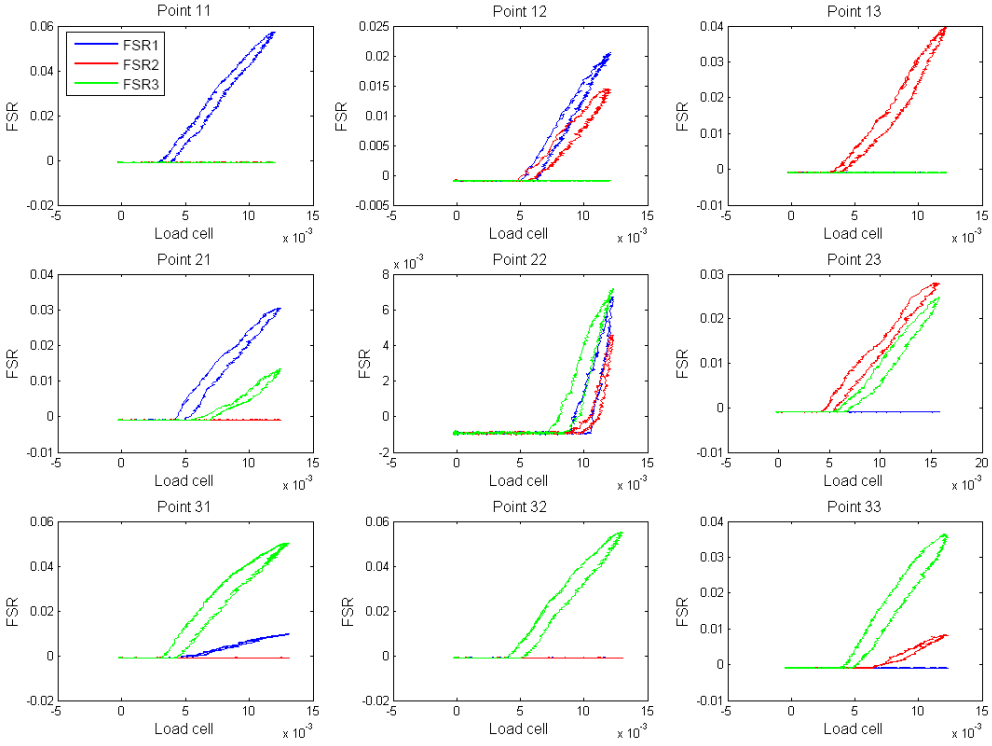

Figure 22: Relationship FSRs and applied pressure

[1]Denomination of the y-axis on all figures in this section: V*. As described in section 6.2, the signals from the FSRs and the load cell gets weaker (still in proportion to each other) as a consequence of the terminators attached to the BNC-plugs. Hence, V* is the resulting voltage [V].

8.1.2 Polynomial curve fitting, second degree

Polynomials can be fitted to the characterization plots in the previous section (FSR-curves). This is done for each one of the characterization points.

The Matlab file `curvefit.m` in Appendix A.1 makes use of the functions `polyfit` and `polyval`. `polyfit(x,y,n)` finds the coefficients of a polynomial $p(x)$ of a given degree n that fits a data set ($p(x(i))$ to $y(i)$) in a least squares sense. The result is a row vector of length (n+1) containing the polynomial coefficients in descending powers. `polyval` returns the value of a polynomial of degree n evaluated at x, in this case `polyval` returns the polynomial of the FSR outputs, as function of the load cell (x).

The second degree polynomials are plotted in Figure 23 (close-up of the curves in Appendix C.1).

$$p_n(x) = a_1x^2 + a_2x + a_3 \tag{12}$$

In Appendix C.1 (equations 18 to 26) are the values of the second degree polynomial $p_n(x)$ (equation 12) for each characterization point given (first row in matrix: FSR1, second row: FSR2, third row: FSR3).

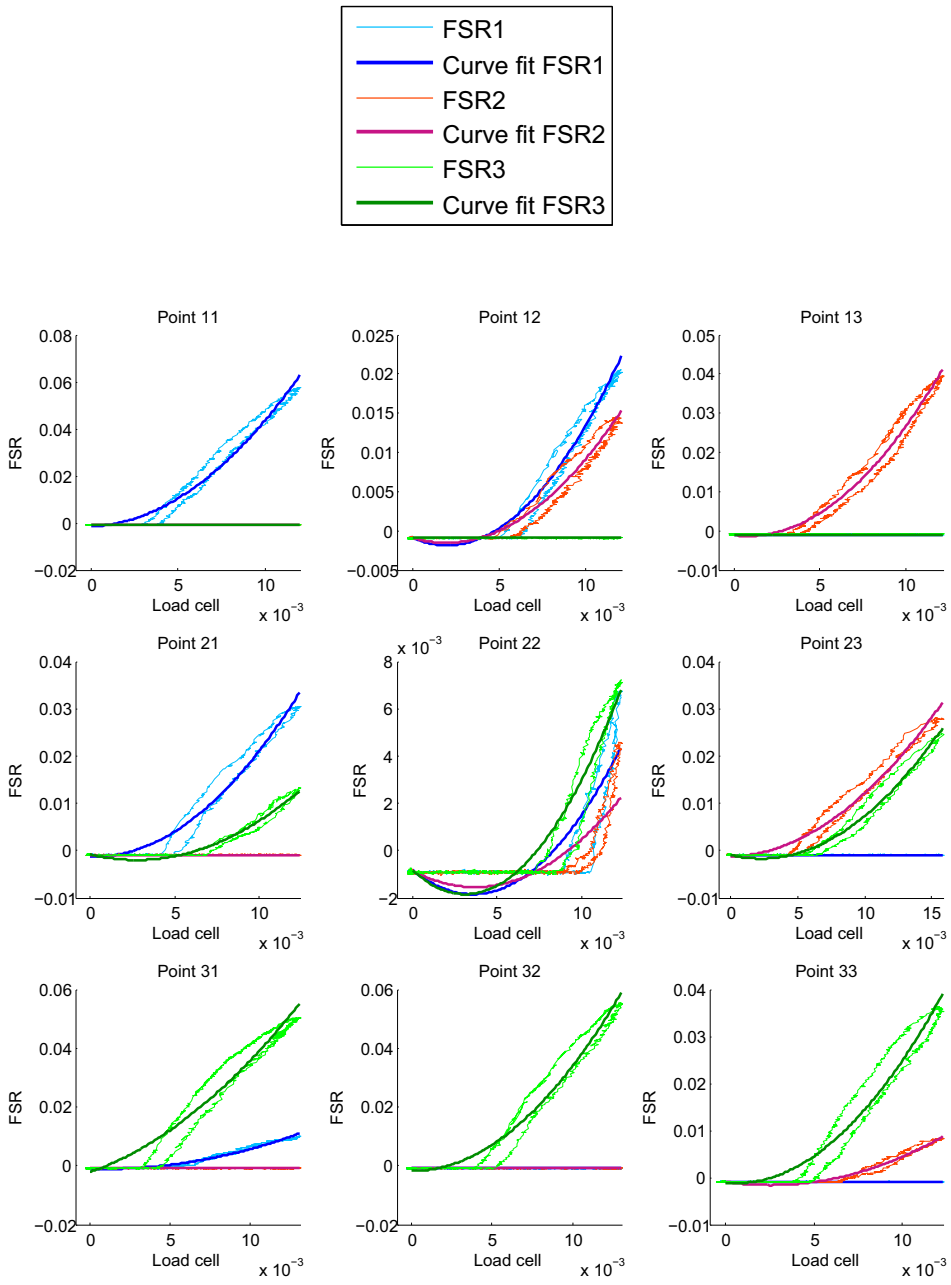

Figure 23: Polynomial curve fitting, second degree

8.1.3 Polynomial curve fitting, third degree

The last argument in the function `polyfit(x,y,n)` is changed from two to three. The third degree polynomials are showed in Figure 24 (close-up of the curves in Appendix C.2).

$$p(x) = b_1 x^3 + b_2 x^2 + b_3 x + b_4 \tag{13}$$

$$\vec{p} = B_{point} \begin{bmatrix} x^3 \\ x^2 \\ x \\ 1 \end{bmatrix} \tag{14}$$

In Appendix C.2 (equations 27 to 35) are the values of the B matrix in equation 14 given (for each point).

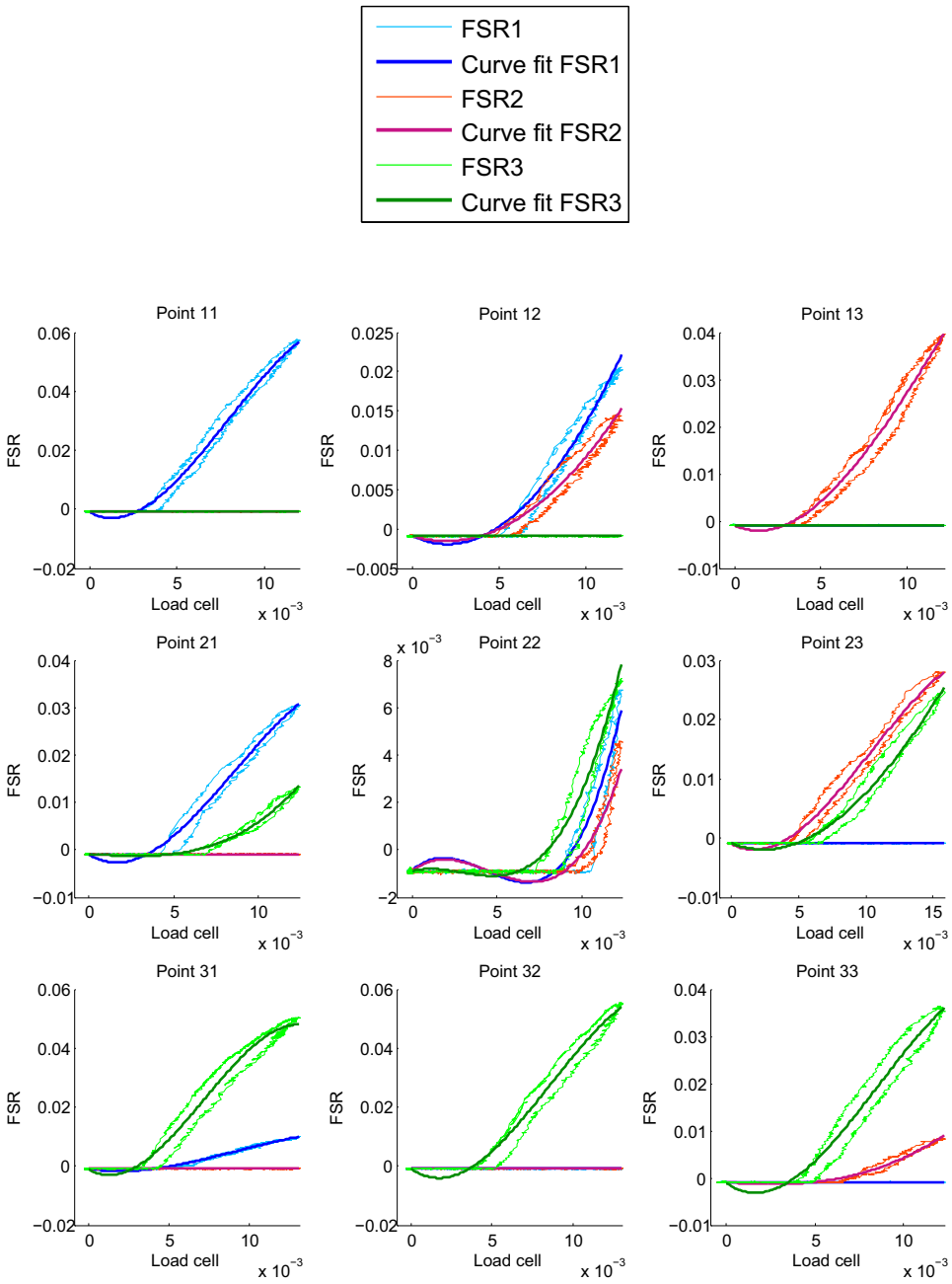

Figure 24: Polynomial curve fitting, third degree

8.2 Muscle force estimation

For each test procedure (presented in section 7), three different data sets were recorded.

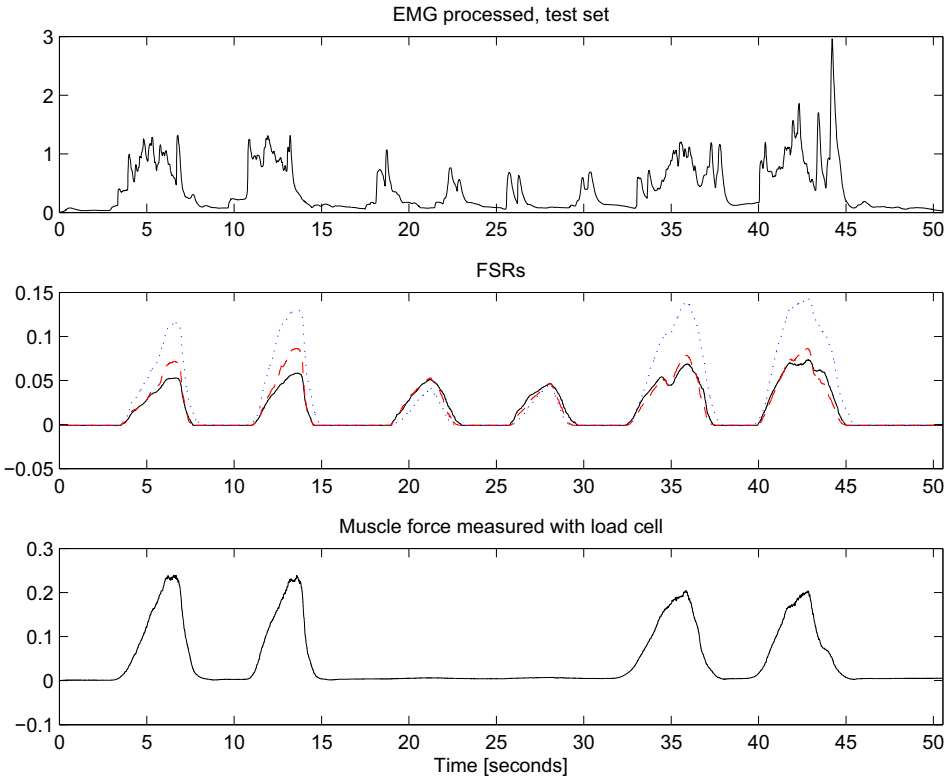

Figure 25: Test set containing measurements from EMG, 3 FSRs and the load cell.

Figure 25 shows the output from the surface electrode, the FSRs and the load cell in the test set (similar curves for the training and validation set). Compare with Figure 21 in section 7. Between ∼17.5 seconds and ∼32.5 seconds (in the processed EMG plot), motion artifacts can clearly be seen. It looks like four action potentials, but in reality, this is just the surface electrode being forced against the skin by external forces (the test subject relaxing).

8.2.1 Linear mapping function (LF)

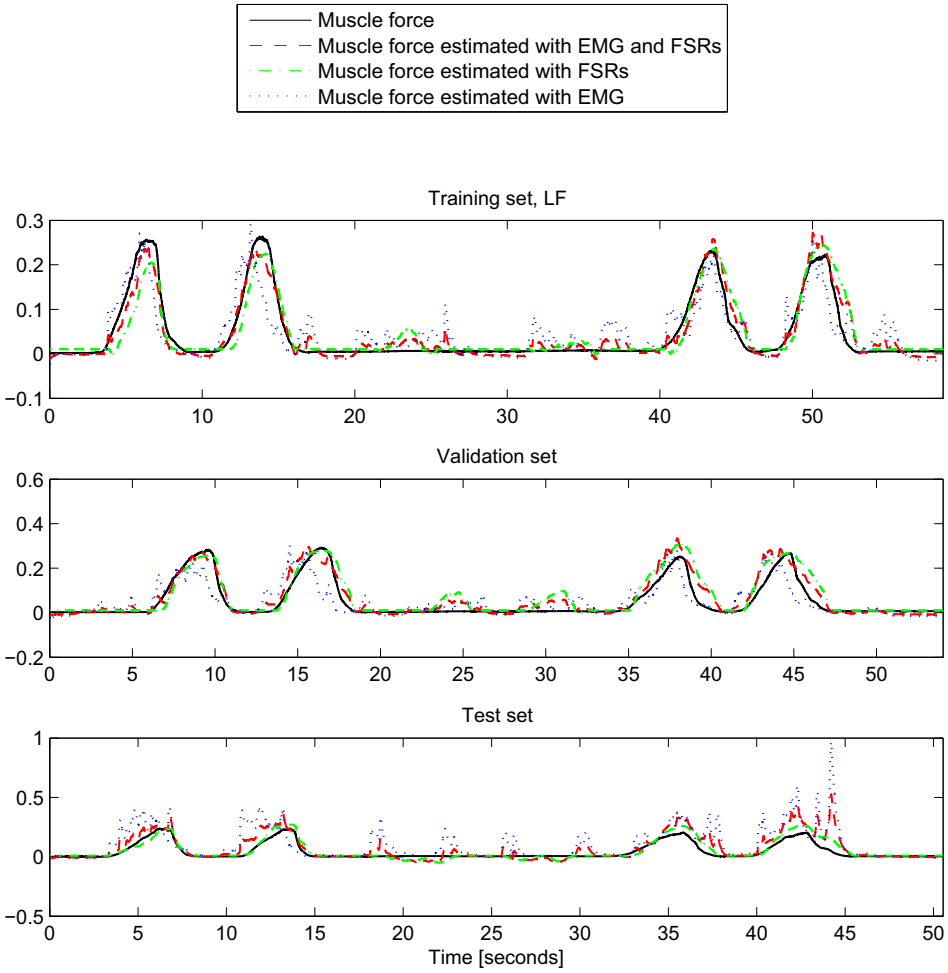

Figure 26: Force estimation with 1st order discriminant function

Estimation with the 1st order discriminant function is plotted in Figure 26[2]. The figure compares the estimation results for the training set, validation set and the test set.

The LF are not a learning method, the estimation procedure is identical repeatedly. This meaning the data sets do not depend on each other, one data set is required for estimation, and there is no need for validation.

[2]Three different data sets are plotted, this is why the limits on the x-axis are varying in the three plots.

8.2.2 Quadratic mapping function (QF)

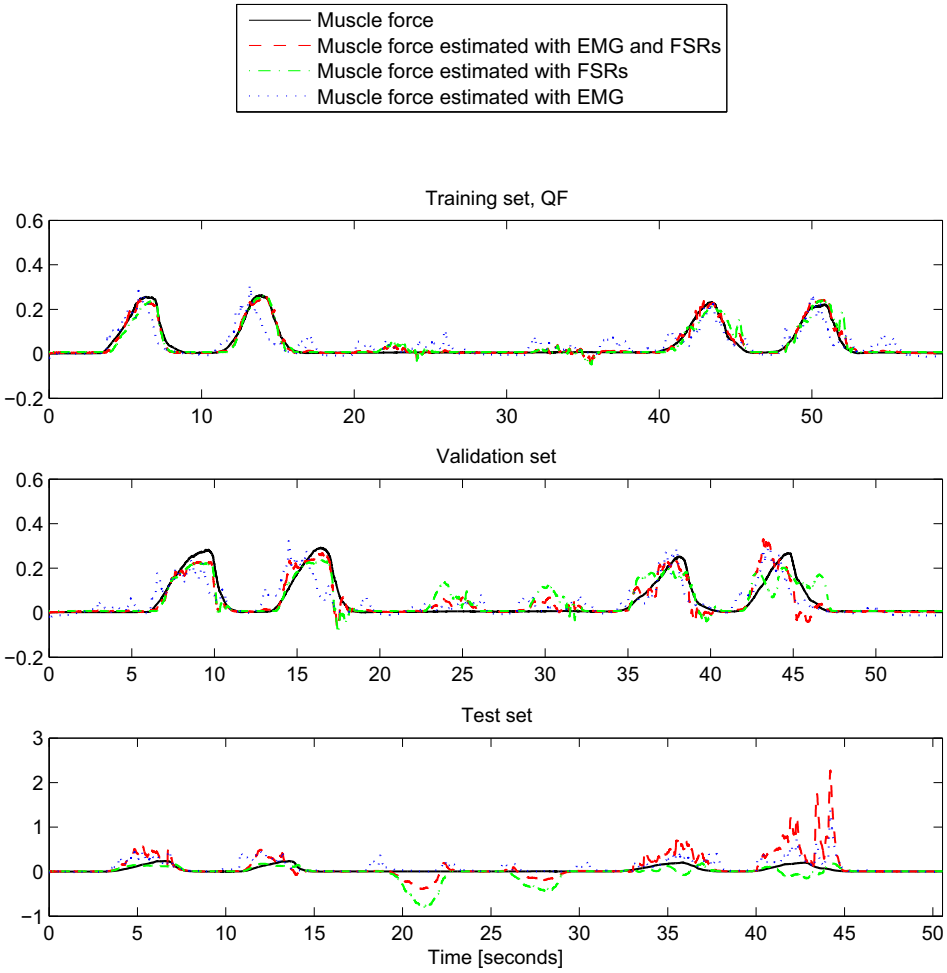

Figure 27: Force estimation with 2nd order discriminant function

Force estimates from the quadratic mapping function are plotted in Figure 27. The figure compares the estimation results for the training set, validation set and the test set. The QF produces good estimates for the training set, but on the other two sets (especially the test set), the QF gives poor estimates. The part where the motion artifacts occur (see Figure 25), the QF actually overcompensates, resulting in negative force estimates (test set in Figure 27).

8.2.3 Multi-layer perceptron network

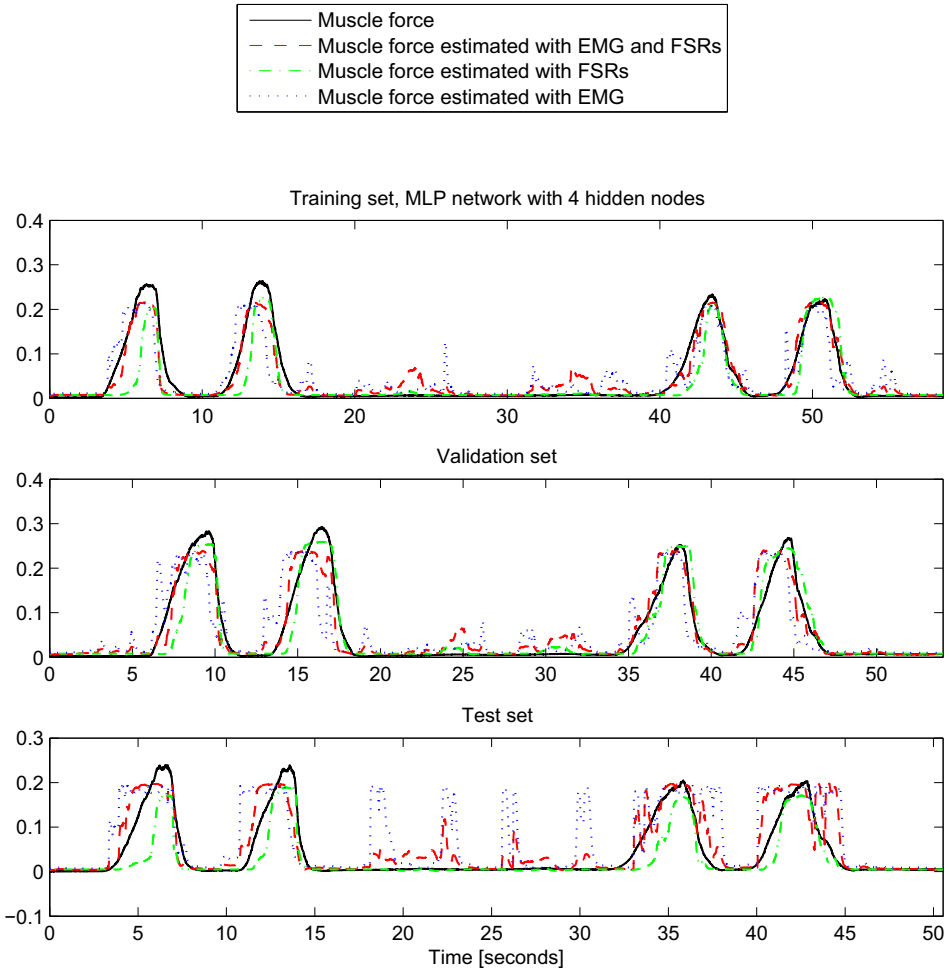

Figure 28: MLP network with 4 hidden nodes

Estimation has been done with 2, 3, 4, 5, 8, 10, 12, 15, 20 and 25 hidden nodes. Estimation of muscle force with MLP networks (3, 8, 15 and 25 hidden nodes) can be seen in Appendix D. Plots of all estimations are put on the CD in Appendix E (E.3, in the folder 2008-05-29-Recordings). Figure 28 shows estimation with four hidden nodes (least RMS error when MLP networks are used for estimation, see 8.2.5). The figure compares the estimation results for the training set, validation set and the test set.

The red line shows the estimated force with both FSR signals and sEMG signals as input signals to the MLP network. Compared to only using sEMG as input, the cancellation of motion artifacts are better, but the general force estimation is not good enough.

8.2.4 Force vs. estimated force

Measured force (from the load cell) plotted vs. estimated force are presented in Figures 29, 30 and 31 (all data sets).

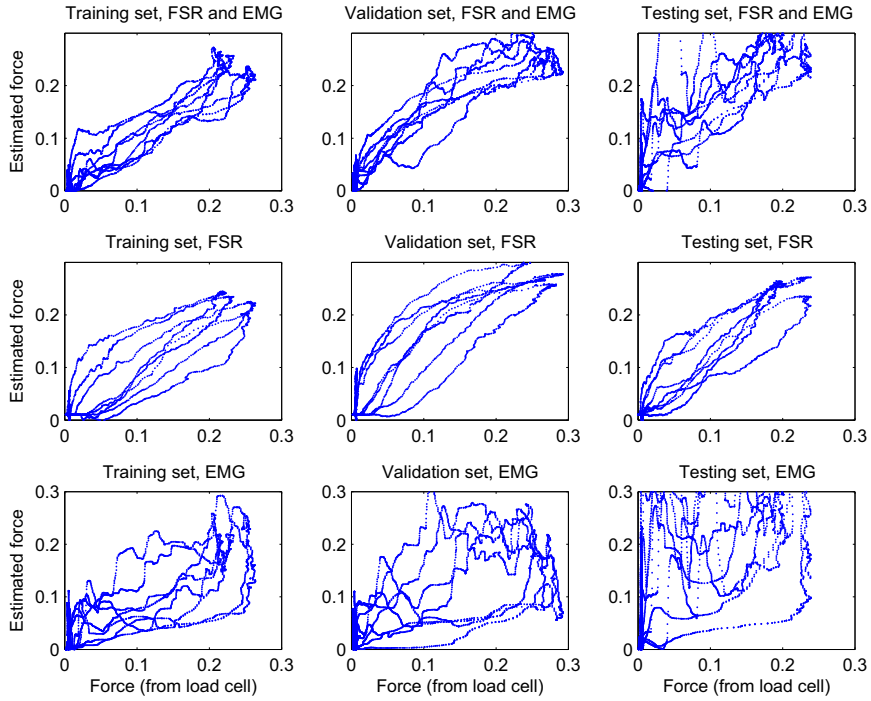

Figure 29: Force vs. estimated force, LF

Figure 30 clearly shows that the QF has been overtrained (special adjusted to the training set). The plot in the upper left corner of the figure indicates an almost linear relationship between estimated force (with FSR and EMG) and real muscle force. This is exactly what is wanted, but the plot in the upper right corner in the same figure shows large scattering of the estimates, this indicates poor linear relation between estimated- and real force for the testing set.

The pattern when FSR signals are used as input shows exactly the same shape of the curves in the characterization, the hysteresis loop. This is a classic feature with the FSRs. This shape tells us that the FSRs only, will not give accurate enough estimates.

Close to the origin in these plots (FSR as input), a peak can clearly be seen. This is force estimates caused by motion artifacts.

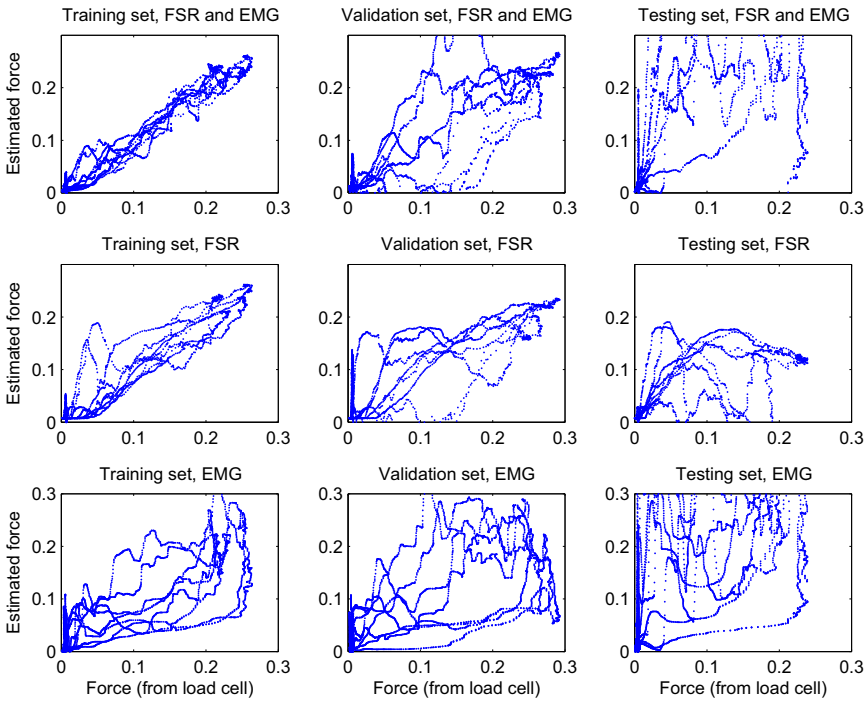

Figure 30: Force vs. estimated force, QF

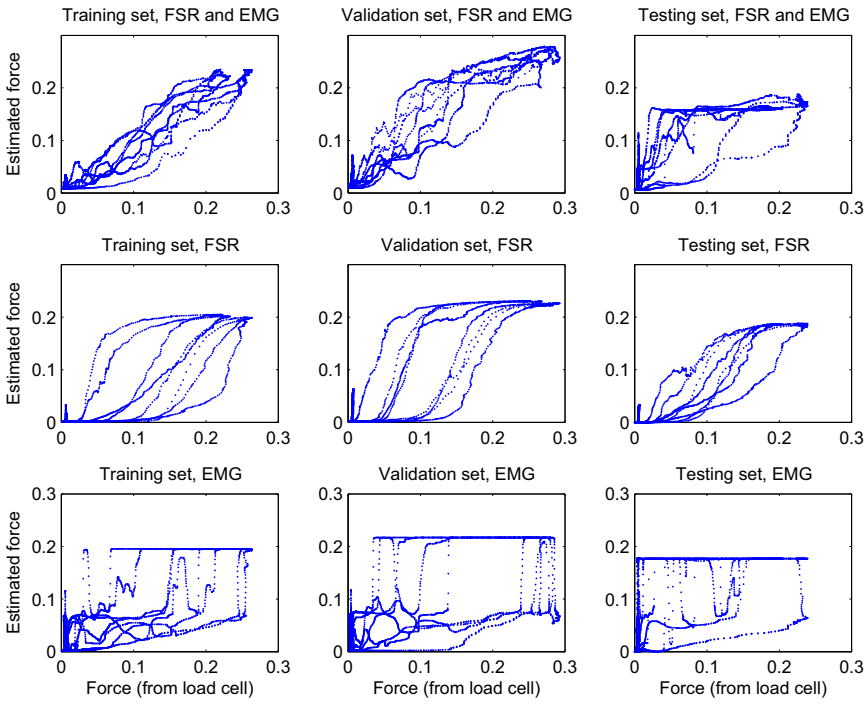

Figure 31: Force vs. estimated force, 4 hidden nodes

8.2.5 Root mean square (RMS) error

The RMS error values on the test set are presented in Figure 32.

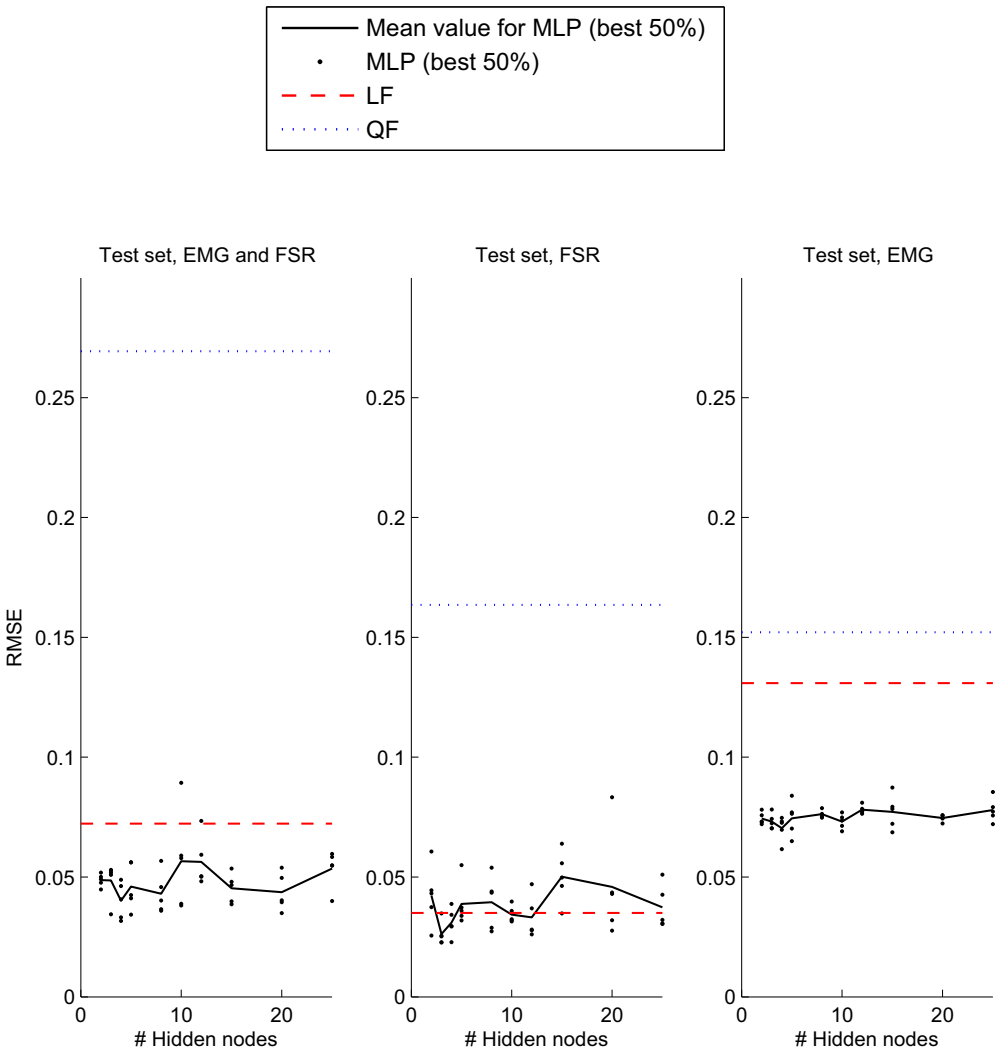

Figure 32: RMSE test set

The RMS error should be expressed as the percentage of the maximum voluntary contraction (MVC). This is achieved by having the test subject attempting to lift the hand upwards with as much force as possible, this value is read off Figure 25. MVC = $\sim$ 0.24 V*.

The red line presents the RMS error for the linear mapping function, the blue dotted line presents RMS error for the quadratic mapping function. The values of the RMS error when using LF and QF for the test set are presented in table 2. The RMS errors when including FSR measurements are 30% (FSR and EMG) and 15% (FSRs only) compared to 55% of the MVC when only using EMG signals in the estimation.

Input	LF [V*]	LF [% of MVC]	QF [V*]	QF [% of MVC]
FSR & EMG	0.072299	∼30	0.26939	∼112
FSR	0.035019	∼15	0.16352	∼68
EMG	0.13091	∼55	0.15216	∼63

Table 2: RMS error, Linear- and quadratic mapping functions (test set)

For each number of hidden nodes (2, 3, 4, 5, 8, 10, 12, 15, 20 and 25), the training process is accomplished ten times. The five MLP networks that perform best on the validation set are selected and plotted (the networks that give zero output or only square pulses are rejected).

In table 3, the best mean values of the RMS errors for the different inputs are presented. The optimal number of hidden nodes is also given. See Figure 32. The lowest RMS error (11% of MVC) appears when estimation is done by a MLP network with FSRs in the input layer, and three hidden nodes. When both EMG and FSR signals are used as input to the MLP network (four hidden nodes), the RMS error is 17% of MVC. Both these numbers are improved compared to only using EMG as input (29% of MVC, four hidden nodes).

Input	RMSE [V*]	RMSE [% of MVC]	# hidden nodes
FSR & EMG	0.040124	∼17	4
FSR	0.0262217	∼11	3
EMG	0.070383	∼29	4

Table 3: RMS error, best mean value MLP network

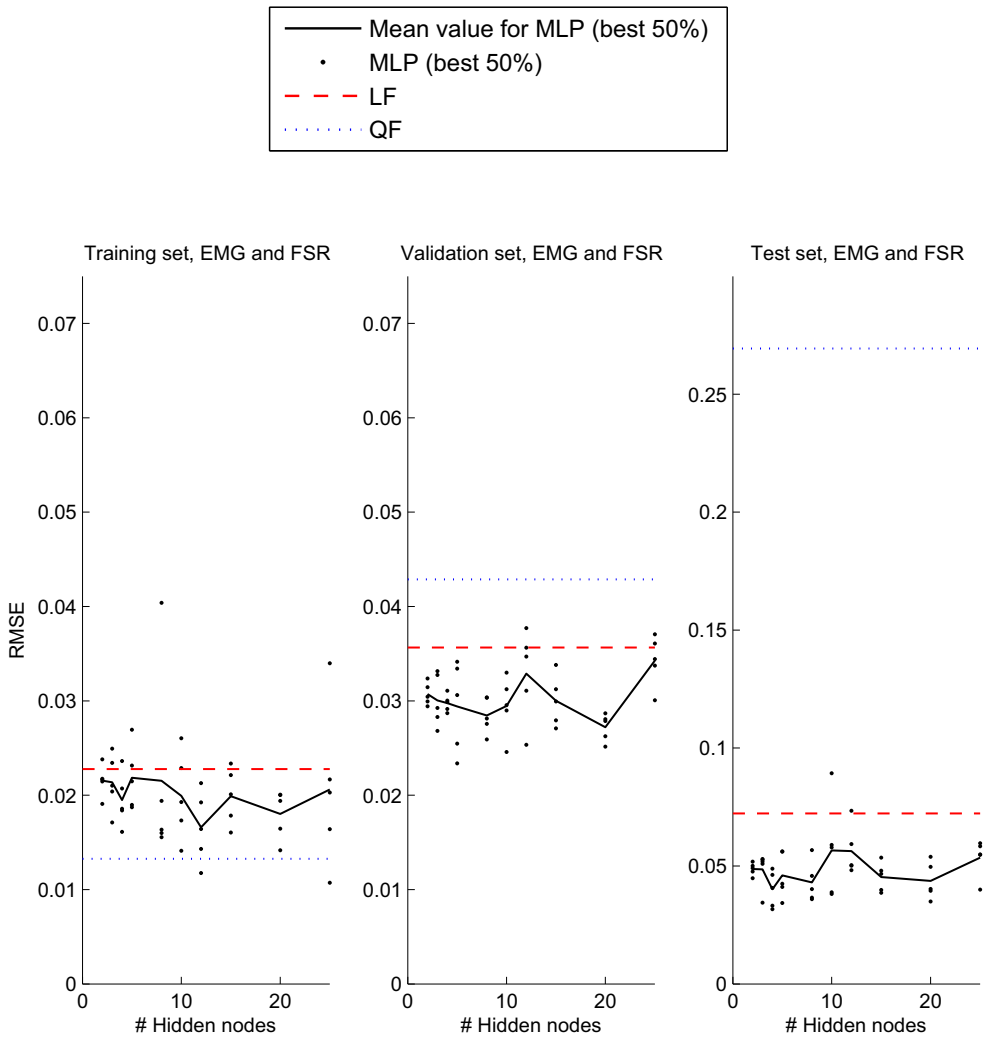

Figure 33: RMS error, EMG and FSR

Figure 33 give an explanation on why the RMS error on the quadratic mapping function (QF) plotted in Figure 32 gets such a high value. The QF gets the lowest RMS error on the first data set (training set) in all the estimation methods. Comparing the plots for the different sets in Figure 33 indicates overtraining of the QF.

9 Discussion

9.1 Characterization of the sEMG sensor

When plotting the FSR outputs as functions of the output from the load cell (Figure 22), the FSR curves get the shape of hysteresis loops. To find curves/-functions that fit the FSR curves (both on the way up and down), polynomial curve fitting has been performed. By comparing e.g. the polynomials for point 22 (the point where all sensors respond to pressure), we can clearly see that the polynomial of third degree makes a better fit than a second order polynomial (close-up of the curves in Appendix C).

A problem occurs at the start of the curve, because the FSRs do not react at once the pressure is applied, they have a threshold. This leading to poor fitting of the polynomials at the start of the curves.

9.1.1 The bias-variance trade off

This is an important issue in data modelling. A model always consists of an architecture and parameters. In polynomial regression (as done in the characterization), the architecture is a polynomial (uniquely identified by its degree) and the parameters are the coefficients of the polynomial. Once the degree of the polynomial is decided, fitting the model consists in finding the appropriate values of the parameters. In this study, the least-squares approach has been used. In polynomial regression, a polynomial with too few parameters (too low a degree) will make large errors because of a large bias, a polynomial with too many parameters (too high a degree) will make large errors because of a large variance. An "overfitted" model may appear to be performing well, in reality it follows the data too closely and will perform poorly on new data.

Identifying the best model requires identifying the proper number of parameters, not too few nor too many. A third degree polynomial seems to be a good enough choice in the characterization case. (The Matlab program `curvefit.m` is put on the CD in Appendix E. The last argument in the function `polyfit` is the degree of the polynomial, to see how higher degree polynomials fit- change this.)

9.2 The mapping functions

The linear mapping function seems to give good estimates of muscle force, and there is more cancellation of the motion artifacts when including the FSR signals in the estimation.

Comparing the training sets in Figures 26 and 27, QF performs better than LF, however LF performs best on the validation- and test sets. This indicates overtraining of the QF (special adjusted to the training set, or overfitted as described in previous subsection).

This indicates that these tests do not reveal if QF is suited for force estimation. Several test procedures have to be accomplished. In theory, QF should perform better than LF.

9.3 MLP network

A multilayer perceptron (MLP) network was employed to estimate the muscle force based on sEMG and FSR signals. Estimation has been done with 2, 3, 4, 5, 8, 10, 12, 15, 20 and 25 hidden nodes. Following MLP training and validation, the system was tested with a third data set acquired after having removed and then reapplied the device to the test subject's arm. The estimated force was then compared to the "true" force measured with the load cell. A qualitative comparison reveals obvious improvements for the sEMG sensor when FSR measurements are included.

When applying external forces to the sensor while the test subject relaxes, the control of the prosthesis should not be influenced. This is the main focus in this study; cancellation of the effect motion artifact have on the control signal. In Figure 34 a segment of estimation with five hidden nodes (test set) is showed. These peaks are force estimates resulting from motion artifacts caused

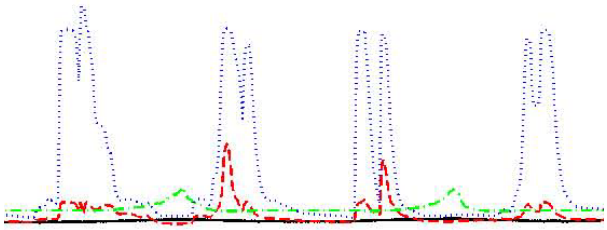

Figure 34: Motion artifacts

by the force applied to the sensor, and the goal is to cancel these signals. None of the methods cancel the artifacts entirely, but the output signal/estimated force signal (control signal for the prosthesis) when using both sEMG and FSR signals as input (red line) reveals obvious improvements compared to using only sEMG as input (blue dotted line). The green line shows muscle force estimated with only FSR signals as input. This estimation gives the best output, however in practice, it can be difficult to carry this through. The main reason for this is the hysteresis behaviour of the FSRs.

It is a goal to keep the number of nodes low in the hidden layer. The advantage of this is that the disturbance/noise gets less and the result is more general, not an overtrained network. In Appendix D, estimations done with 3, 8, 15 and 25 hidden nodes are showed. The estimated force gets more noisy the more nodes in the hidden layer.

The training method of Matlab's Neural Network Toolbox stops training when the error for the validation set starts to increase (divergence of the result). If the validation set is too different from the training set, the training procedure terminates already after the initialization, and the resulting force estimates will only be the initial values (some of the estimated outputs/curves

becomes flat).

For each number of hidden nodes (2, 3, 4, 5, 8, 10, 12, 15, 20 and 25), the training process have been accomplished ten times. The five MLP networks that perform best on the validation set are selected for further examination. In reality, training should be performed in a more extreme manner, e.g 1500 times, and the for instance 10 networks that perform best are chosen for testing. Then a prosthesis user may test the different networks, and the one that best adapts to the user/the user adapts best to, is implemented in the prosthesis control. And finally, more testing of the prosthesis is required in the daily life.

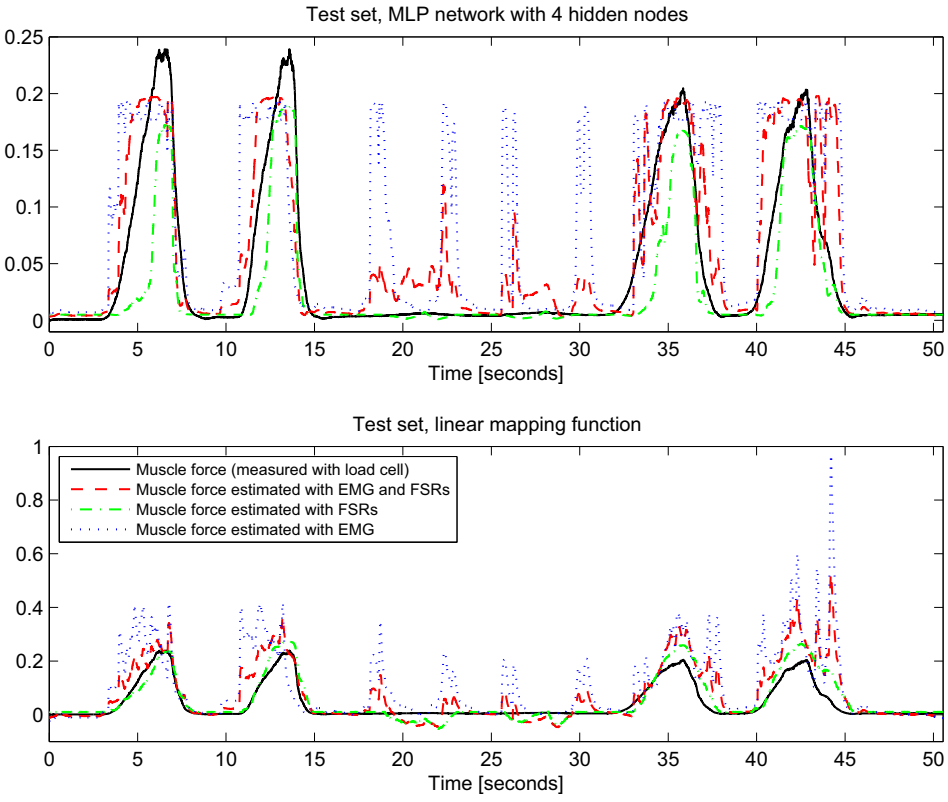

Figure 35: Comparison between MLP and LF

If estimation method should be chosen based directly from the estimates done in this study, LF would most likely be chosen ahead of MLP network (according to Figure 35). In reality, the negative force estimated by the LF, is hard to understand how can be accomplished. A lot more testing (both on the laboratory and in a real prosthesis socket on the residual limb of an amputee) are required before selecting estimation method.

9.3.1 F vs. F_e

Measured force (from the load cell) plotted vs. estimated force (four hidden nodes) are presented in Figure 31 in section 8. The pattern when FSR signals

are used as input shows exactly the same shape of the curves in the characterization, the hysteresis loop.

Ideally the relationship between measured muscle force and estimated muscle force should be linear (then the error $e_j = (F_j - \hat{F}_j)$ will be minimized). This is not accomplished, but comparing the plots when using only EMG and using both EMG and FSRs, reveals an improvement in the latter case. Figure 36 shows muscle force plotted vs. estimated force for all test sets.

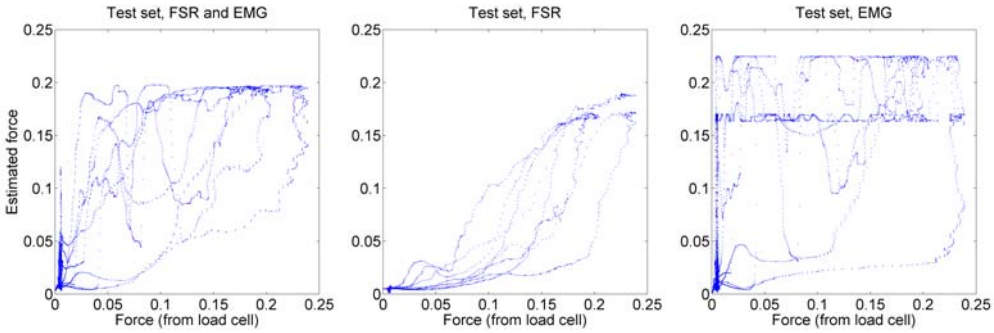

Figure 36: Force vs. estimated force

When EMG is used as input, upper thresholds can be seen in the figure (See also the figures in section 8.2.4). These thresholds indicate that in practice, the prosthesis will function well up to a certain point and when this threshold is reached, unsolicited behaviour will occur. The reason for this threshold may be the shape of the real force curve (See Figure 25). The muscle force from the user are performed in a dynamic manner, first easy contraction, then relaxing (this looks like a square pulse). The sEMG varies a lot more than this, and the difference between the sEMG and the wanted estimated force gets large. The training algorithm then gets something to struggle with when training the MLP network. This upper threshold that can be seen is the value when the estimates gets least error. A solution to this problem can be harder filtering of the EMG signal, or varying the muscle force from the test subject even more.

9.4 RMS error

Estimation with MLP network gives the least RMS error (Figure 32). This is not surprising, as the MLP network can act as both LF and QF if that is the optimal estimation method. In that case, the bias-variance trade off is an important issue, it is important to find the optimal number of hidden nodes. This has been done thorough with 2-3-4-5-8-10-12-15-20-25 nodes, and the training procedure is accomplished ten times for each number of nodes. The possibility to get a good MLP network should therefore be high.

MLP network with two, three and four hidden nodes performs well. This have a clear connection to why LF performs better than QF.

When estimation is done by the MLP network, the RMS error gets lower when taking the FSR signals into consideration. For force estimation on the test set with sEMG and FSR signals as input, the RMS error gets least when the

number of hidden nodes are four. With FSR signals as input, lowest RMS error when using three hidden nodes, and when using sEMG as input, the optimal number of nodes is four (See table 3 in section 8).

The actual value of the RMS error is not of importance. What is significant is to try to minimize this error as much as possible, and then test how the user of the prosthesis experience the control of the prosthesis.

10 Conclusion

Artifact cancellation techniques in myoelectric prosthesis control are extremely limited described in the research literature. Hopefully, the sensor developed in this study can be a contribution in the right direction. A sensor that can do simultaneous measurements of sEMG and contact forces between a surface electrode and the skin has been developed, improved and characterized. A protocol has been developed for the recording of the different signals in a laboratory. Suitable data sets have been recorded from one test subject, and pattern recognition methods were employed to estimate the muscle force based on sEMG and FSR signals. The estimated force was then compared to the "true" muscle force measured with a load cell.

A qualitative comparison reveals obvious improvements for the force estimation when FSR measurements are included. The effect motion artifacts have on prosthesis control can, if not cancelled entirely, be reduced when including FSR signals in the estimation of muscle force.

Further research is needed; the sensor should be improved, the MLP networks need more testing to be able to find the optimal number of hidden nodes and the sEMG signal processing needs optimalization. Other artifact cancellation techniques should be tested on the data sets as well. The final step will hopefully be to integrate FSRs in a real prosthesis socket.

11 Suggestions for future work

A more suitable sensor The prototype sEMG sensor made in this study would not fit into a real prosthesis. But with a more appropriate size and shape, the entire device easily fits into a prosthesis socket. The sensor made in this study has proved that the idea of using FSRs to cancel motion artifacts is achievable, and should be further developed.

Noise cancellation The different signals recorded by the sEMG sensor with force measurements are all brought into an adapter (BNC-2090). Wires may be infecting each other, causing noisy signals. Filtering of all signals, or improvement of the laboratory setup should be carried out.

Characterization points Several characterization points should be exposed to external forces to get a more complete characterization of the FSR array.

Position- and external force estimation We want to simulate one sensor with the three FSRs. It should be possible to estimate the position and size of the external force (with an uncertainty) that is applied, from the FSR outputs.

In equation 15, (x, y) is a known position (here should the real coordinates be used (from table 1 in section 7)), F is the external applied known force. The signals s_1, s_2 and s_3 are the measured FSR outputs.

$$\begin{bmatrix} x, y, F \\ \cdots \\ \cdots \end{bmatrix} = \begin{bmatrix} s_1, s_2, s_3 \\ \cdots \\ \cdots \end{bmatrix} \tag{15}$$

$$\begin{bmatrix} F \\ x \\ y \end{bmatrix} = f\left(\begin{bmatrix} FSR1 \\ FSR2 \\ FSR3 \end{bmatrix} \right) \tag{16}$$

A mapping should be done from e.g. equation 17.

$$\begin{bmatrix} F \\ x \\ y \end{bmatrix} = A \begin{bmatrix} s_1 \\ s_2 \\ s_3 \end{bmatrix} + B \begin{bmatrix} s_1^2 \\ s_1 s_2 \\ s_1 s_3 \end{bmatrix} + C \begin{bmatrix} s_1 s_2 \\ s_2^2 \\ s_3 s_2 \end{bmatrix} + D \begin{bmatrix} s_1 s_3 \\ s_2 s_3 \\ s_3^2 \end{bmatrix} \tag{17}$$

To check how well the estimated positions and forces fits the real values, the estimated x-position should be plotted as a function of real x-position (the same should be done for the y-position and force). Ideally this relationship should be linear.

Improvements of pattern recognition methods It exists several pattern recognition methods than described in this thesis. Different methods may give different results, and the search for the best suited method is a topic for further work.

It is important to find the optimal number of hidden nodes. MLP networks are never identical because of varying initial values, and applying some averaging or other statistics (more extrema than five out of ten) on several trained MLP networks could be a solution.

Explore several muscles To get more accurate estimates of the muscle force, more muscles than biceps brachii should be taken into account. To start with, at least some of the muscles on the backside of the arm.

Other artifact cancellation methods A large, suitable data set from the laboratory are available. The sensor is also available at the laboratory, and more data acquisition can be performed. Other methods for "Artifact-free force estimation" based on mathematical models describing the correspondence between physical movements/forces and the resulting sEMG artifacts should be searched for.

Realization A prosthesis socket with either FSRs or strain gauges should be constructed, and more testing and recordings should be performed. Training should be done on a lot of data, validation on e.g. half of the data, and finally (and hopefully), the system can be implemented in real prosthesis control. Then testing can be done by a prosthesis user.

12 Bibliography

John V. Basmajian and Carlo J. DeLuca. *Muscles Alive, Their Functions Revealed by Electromyography*. Williams & Wilkins, fifth edition edition, 1985.

E. A. Clancy, E. L. Morin, and R. Merletti. Sampling, noise-reduction and amplitude estimation issues in surface electromyography. *Journal of Electromyography and Kinesiology*, 12:1–16, 2002.

Digitimer. Digitimer homepage, May 12 2008. URL `http://www.digitimer.com/`.

S. Ödman and P. Aake Öberg. Movement-induced potentials in surface electrodes. *Medical & Biological Engineering and Computing*, 20:159–166, 1982.

John Enderle, Susan M. Blanchard, and Joseph Bronzino. *Introduction to Biomedical Engineering 2Ed.* Academic Press, 2006.

Anders Lyngvi Fougner. Proportional myoelectric control of a multifunction upper-limb prosthesis. Master's thesis, Norwegian University of Science and Technology, 2007.

Patrick S. Hamilton and Michael G. Curley. Adaptive removal of motion artifact. In *Proceedings - 19th International Conference*, 1997.

HBM. Waegezelle z6fc3, May 26 2008. URL `http://www.hbm.com/en/menu-top/home/`.

InterlinkElectronics. Interlink electronics homepage, April 15 2008. URL `http://www.interlinkelectronics.com/`.

Philipp Kampas. The optimal use of myoelectrodes. *Med. Orth. Tech*, 1:21–26, 2001.

Yan Liu and Michael G. Pecht. Reduction of skin stretch induced motion artifacts in electrocardiogram monitoring using adaptive filtering. In *Proceedings of the 28th IEEE EMBS Annual International Conference*, 2006.

G. De Luca, S. H. Roy, S. Cheng, P. Bergman, A. Johansson, D. Gilmore, and C.J. De Luca. Electro-mechanical stability of surface emg sensors. *Delsys*, 2006.

Torunn Margrete Midtgaard. Advanced myoelectric control of a multifunction upper-limb prosthesis. Master's thesis, Norwegian University of Science and Technology, 2006.

Ashok Muzumdar. *Powered Upper Limb Prostheses*, chapter 3. Springer-Verlag Berlin Heidelberg New York, 2004a.

Ashok Muzumdar. *Powered Upper Limb Prostheses*. Springer-Verlag Berlin Heidelberg New York, 2004b.

NationalInstruments. National instruments homepage, May 12 2008. URL `http://www.ni.com/`.

T. Okamoto, H. Tsutsumi, Y. Goto, and P. D. Andrew. A simple procedure to attenuate artifacts in surface electrode recording by painlessly lowerin skin impedance. *Electromyo. & Clin. Neurophysiol.*, 27:173–176, 1987.

P.A. Parker, K.B. Englehart, and B.S. Hudgins. *Control of Powered Upper Limb Prostheses*, chapter 18. P.A. Parker, 2004.

Lennart Philipson and Pål G. Larsson. *The electromyographic signal used for control of upper extremity prostheses and for quantification of motor blockade during epidural anaesthesia - The electromyographic signal as ameasure of muscular force: A comparison of detection and quantification techniques*. PhD thesis, Linköping University, 1987.

Martin Risdal. *Impedance pethysmography for ventilation and pulse monitoring during cardiopulmonary resuscitation*. PhD thesis, University of Stavanger, 2006.

Rod R. Seeley, Trent D. Stephens, and Philip Tate. *Essentials of Anatomy & Physiology*, chapter 7, pages 156–187. McGraw-Hill, 2007.

SensorWiki. Sensorwiki, May 23 2008. URL `http://www.sensorwiki.org/index.php/Force-sensitive_resistor_(FSR)`.

Marthe Sæther. Artifact cancellation in surface myoelectric signals. Technical report, NTNU, 2007.

Hak W. Tam and John G. Webster. Minimizing electrode motion artifact by skin abrasion. *IEEE Transactions on Biomedical Engineering*, BME-24, NO.2: 134–139, 1977.

D. A. Tong, K. A. Bartels, and K. S. Honeyager. Adaptive reduction of motion artifact in the electrocardiogram. In *Proceedings of the Second Joint EMBS/BMES Conference*, 2002.

www.allaboutcircuits.com. Ohm's law (again!), May 23 2008. URL `http://www.allaboutcircuits.com/vol_1/chpt_3/4.html`.

Øyvind Stavdahl, Åge Grønningsæter, and Kjell Erling Malvig. Ultrasound based estimation of muscle contraction. *Issues in upper-limb prosthetics*, Myoelectric Controls/Powered Prosthetics Symposium:1–6, 1997.

Ping Zhou, Madeleine M. Lowery, Richard F. ff Weir, and Todd A. Kuiken. Elimination of ecg artifacts from myoelectric prosthesis control signals developed by targeted muscle reinnervation. In *Elimination of ECG Artifacts*, 2005.

Ping Zhou, Blair Lock, and Todd A. Kuiken. Real time ecg artifact removal for myoelectric prosthesis control. *Physiological Measurements*, 28:397–413, 2007.

Appendix A Source code from Matlab

All my programs are tested in `MATLAB 7.4.0(R2006a)`. The estimation programs require the `Neural Network Toolbox`.

Appendix A.1 `curvefit.m`

```
clc
clear all
close all

%% Curvefitting, characterisation
% p = polyfit(x,y,n) finds the coefficients of a polynomial p(x) of degree n that fits the data,
% p(x(i)) to y(i), in a least squares sense. The result p is a row vector of length n+1 containing
% the polynomial coefficients in descending powers

% To see how good the fit is, evaluate the polynomial at the data points with f = polyval(p,x);

n = 1;
figure('Name','Curve fitting' ,'NumberTitle','on')
for a = 1:3
    for b = 1:3
        eval(['load ' 'testing' num2str(a)  num2str(b)])

        p2 = polyfit(ans(5,:),ans(2,:),2)
        p3 = polyfit(ans(5,:),ans(3,:),2)
        p4 = polyfit(ans(5,:),ans(4,:),2)

        t2 = 0:0.0001:max(ans(5,:));

        y2 = polyval(p2,t2);
        y3 = polyval(p3,t2);
        y4 = polyval(p4,t2);

        subplot(3,3,n)
        hold on
        plot(ans(5,:),ans(2,:),'Color',[0,0.75,1])
        plot(t2,y2,'b','LineWidth',1.5)
        xlim([-0.0009 max(ans(5,:))])

        plot(ans(5,:),ans(3,:),'Color',[1,0.27,0])
        plot(t2,y3,'Color',[0.78,0.08,0.52],'LineWidth',1.5)
        xlim([-0.0009 max(ans(5,:))])

        plot(ans(5,:),ans(4,:),'g')
        plot(t2,y4,'Color',[0,0.55,0],'LineWidth',1.5)
        xlim([-0.0009 max(ans(5,:))])

        title(['Point ' num2str(a) num2str(b)],'fontsize',10)
        hold off

        n = n + 1;

        xlabel('Load cell','fontsize',10)
        ylabel('FSR','fontsize',10)


    end
end
legend('Location','SouthOutside','FSR1','Curve fit FSR1','FSR2','Curve fit FSR2','FSR3','Curve fit FSR3');
```

Appendix A.2 `FirstOrderEstimation.m`

```
function [F_e,Fval_e,Ftest_e] = firstOrderEstimation(Tdata,Tval,Ttest,N,Xdata,
    Fdata,Xvaldata,Fvaldata,Xtestdata,Ftestdata)
% FIRSTORDERESTIMATION  Calculates first-order parameters W to estimate the
% function F from signals in Xdata using least-squares estimation.
% There are N signals and T time steps.
%
% For every time step we have
% F_e(X) = X'*W+ w0
%
% where
% X = (x1,x2,...,xN), W = (w1,w2,...,wN), w0 is a scalar treshold value
%
% We rewrite it as
% F_e(X) = X'*W+ W_0
%
% where
% X = (1,x1,x2,...,xN), W = (w0,w1,w2,...,wN)
%
% W is found such that we minimize V = 0.5*sum( (F_e(X) - F(X))^2 )
% where X and f(X) are known vectors.
%
% F_e, Fval_e and Ftest_e are then found using W.
%
% Finally, the function returns F_e, which is the estimate of F,
% Fval_e, which is the estimate of Fval, and Ftest_e, which is
% the estimate of Ftest.

% Anders Fougner, anderfo@stud.ntnu.no
% $Revision: 2.0 $Date: 2007/05/20 22:13:00 $

%% Estimation 1st order
% Performing least-squares estimation for each of N signals

% Adjust X
X = [ones(1,Tdata); Xdata]; % add 'ones' for calculating W_0 parameters

%Calculate the optimal W_big containing W, W_0
W = X'\Fdata';

% Calculate F_e(X), the estimate of F(x)
F_e = W'*X;

%% Simulate using validation data
% Adjust Xval
Xval = [ones(1,Tval); Xvaldata]; % add 'ones' for calculating W_0 parameters
% Calculate Fval_e(X), the estimate of Fval(x)
Fval_e = W'*Xval;

%% Simulate using test data
% Adjust Xtest
Xtest = [ones(1,Ttest); Xtestdata]; % add 'ones' for calculating W_0
    parameters
% Calculate Fval_e(X), the estimate of Fval(x)
Ftest_e = W'*Xtest;
```

Appendix A.3 SecondOrderEstimation.m

```
function [F_e,Fval_e,Ftest_e] = secondOrderEstimation(Tdata,Tval,Ttest,N,Xdata
    ,Fdata,Xvaldata,Fvaldata,Xtestdata,Ftestdata)
% FIRSTORDERESTIMATION  Calculates second-order parameters W to estimate
% the function F from signals in Xdata using least-squares estimation.
% There are N signals and T time steps.
%
%
% For every time step we have
%
% F_e(X) = X'*W2*X + W1'*X + w0
%
% where
% X = (x1,x2,...,xN), W1 = (w1,w2,...,wN), w0 is a scalar treshold value
% and
%       |w11 ... w1N|
% W2 =  |... ... ...|
%       |wN1 ... wNN|
%
%
% We rewrite it as
%
% F_e(X) = W*X
%
% where
% X = ( 1;   x1:xN;   x1x1:xNxN;   x1x2:x(N-1)xN;   x1x3:x(N-2)xN; ... )
% W = (w0,   w1:wN,   w11:wNN,     w12:w(N-1)N,     w13:w(N-2)N    ... )
%
% W should be found such that we minimize V = 0.5*sum( (f_e(X) - f(X))^2 )
% where X and f(X) are known vectors.
%
% F_e, Fval_e and Ftest_e are then found using W.
%
% Finally, the function returns F_e, which is the estimate of F,
% Fval_e, which is the estimate of Fval, and Ftest_e, which is
% the estimate of Ftest.

% Anders Fougner, anderfo@stud.ntnu.no
% $Revision: 2.0 $Date: 2007/05/20 22:13:00 $

%% Estimation 2nd order
% Performing least-squares estimation for each of N signals

% Adjust X
X = [ones(1,Tdata)]; % add 'ones' for calculating W_0 parameters
X = [X; Xdata];
% The for-loop goes on like this:
% X = [X;(Xdata(1:N,1:T).*Xdata(1:N,1:T))];
% X = [X;(Xdata(1:N-1,1:T).*Xdata(2:N,1:T))];
% X = [X;(Xdata(1:N-2,1:T).*Xdata(3:N,1:T))];
% ...
% X = [X;(Xdata(1:1,1:T).*Xdata(N:N,1:T))];
for k=N:-1:1
    X = [X;(Xdata(1:k,1:Tdata).*Xdata(N-k+1:N,1:Tdata))];
end

%Calculate the optimal W
W = X'\Fdata';

% Calculate F_e(X), the estimate of F(x)
F_e = W'*X;

%% Simulate using validation data
% Adjust Xval in the same way as X was adjusted
Xval = [ones(1,Tval)]; % add 'ones' for calculating W_0 parameters
```

```
64 Xval = [Xval; Xvaldata];
65 for k=N:-1:1
66     Xval = [Xval;(Xvaldata(1:k,1:Tval).*Xvaldata(N-k+1:N,1:Tval))];
67 end
68
69 % Calculate Fval_e(X), the estimate of Fval(X)
70 Fval_e = W'*Xval;
71
72 %% Simulate using test data
73 % Adjust Xtest in the same way as X was adjusted
74 Xtest = [ones(1,Ttest)]; % add 'ones' for calculating W_0 parameters
75 Xtest = [Xtest; Xtestdata];
76 for k=N:-1:1
77     Xtest = [Xtest;(Xtestdata(1:k,1:Ttest).*Xtestdata(N-k+1:N,1:Ttest))];
78 end
79
80 % Calculate Ftest_e(X), the estimate of Ftest(X)
81 Ftest_e = W'*Xtest;
```

Appendix A.4 neuralNetwork.m

```
function [F_e,Fval_e,Ftest_e] = neuralNetwork(Tdata,Tval,Ttest,Nx,Nf,Xdata,
    Fdata,Xvaldata,Fvaldata,TfChoice,HiddenNodes,Xtestdata,Ftestdata)
% FIRSTORDERESTIMATION  Uses neural network theory to find a relation
% between a signal matrix X (for N signals and T time steps) and a function
% matrix F.
% Then it generates an estimate F_e of the function matrix F, using the
% neural net.
%
% Finally, the function returns F_e, which is the estimate of F, and
% according results for validation and test sets.

% Anders Fougner, anderfo@stud.ntnu.no
% $Revision: 2.0 $Date: 2007/05/20 22:13:00 $


% "Normalization/standardization" of output data
[Fdata2,FdataS] = mapminmax(Fdata);
[Fvaldata2,FvaldataS] = mapminmax(Fvaldata);
[Ftestdata2,FtestdataS] = mapminmax(Ftestdata);

% Choice of transfer function in the nodes/synapses of the NN
Tfs(1:HiddenNodes,1:Nf) = {TfChoice}; % tansig is default
disp(['Using ' num2str(HiddenNodes) ' nodes in the hidden layer.']);

%% Adjust X to 2nd degree
% X = Xdata;
% for k=Nx:-1:1
%     X = [X;(Xdata(1:k,1:Tdata).*Xdata(Nx-k+1:Nx,1:Tdata))];
% end
%% Adjust Xval in the same way as X was adjusted
% Xval = Xvaldata;
% for k=Nx:-1:1
%     Xval = [Xval;(Xvaldata(1:k,1:Tval).*Xvaldata(Nx-k+1:Nx,1:Tval))];
% end
%% Adjust Xtest in the same way as X was adjusted
% Xtest = Xtestdata;
% for k=Nx:-1:1
%     Xtest = [Xtest;(Xtestdata(1:k,1:Ttest).*Xtestdata(Nx-k+1:Nx,1:Ttest))];
% end

% Generate a neural network
net = newff(minmax(Xdata),[HiddenNodes Nf],Tfs);

% Make validation and testing structures
VV.P = Xvaldata;
VV.T = Fvaldata2;
TV.P = Xtestdata;
TV.T = Ftestdata2;

% Train the neural network, but do not print error messages
net.trainParam.show = NaN;
[net,tr]=train(net,Xdata,Fdata2,[],[],VV,TV);

% Simulate Xdata and Xvaldata in the NN to estimate F and Fval
F_e = sim(net,Xdata);
Fval_e = sim(net,Xvaldata);
Ftest_e = sim(net,Xtestdata);

% "Denormalization/unitization" of output data
F_e = mapminmax('reverse',F_e,FdataS);
Fval_e = mapminmax('reverse',Fval_e,FvaldataS);
Ftest_e = mapminmax('reverse',Ftest_e,FtestdataS);
```

Appendix B Simulink model, signal processing

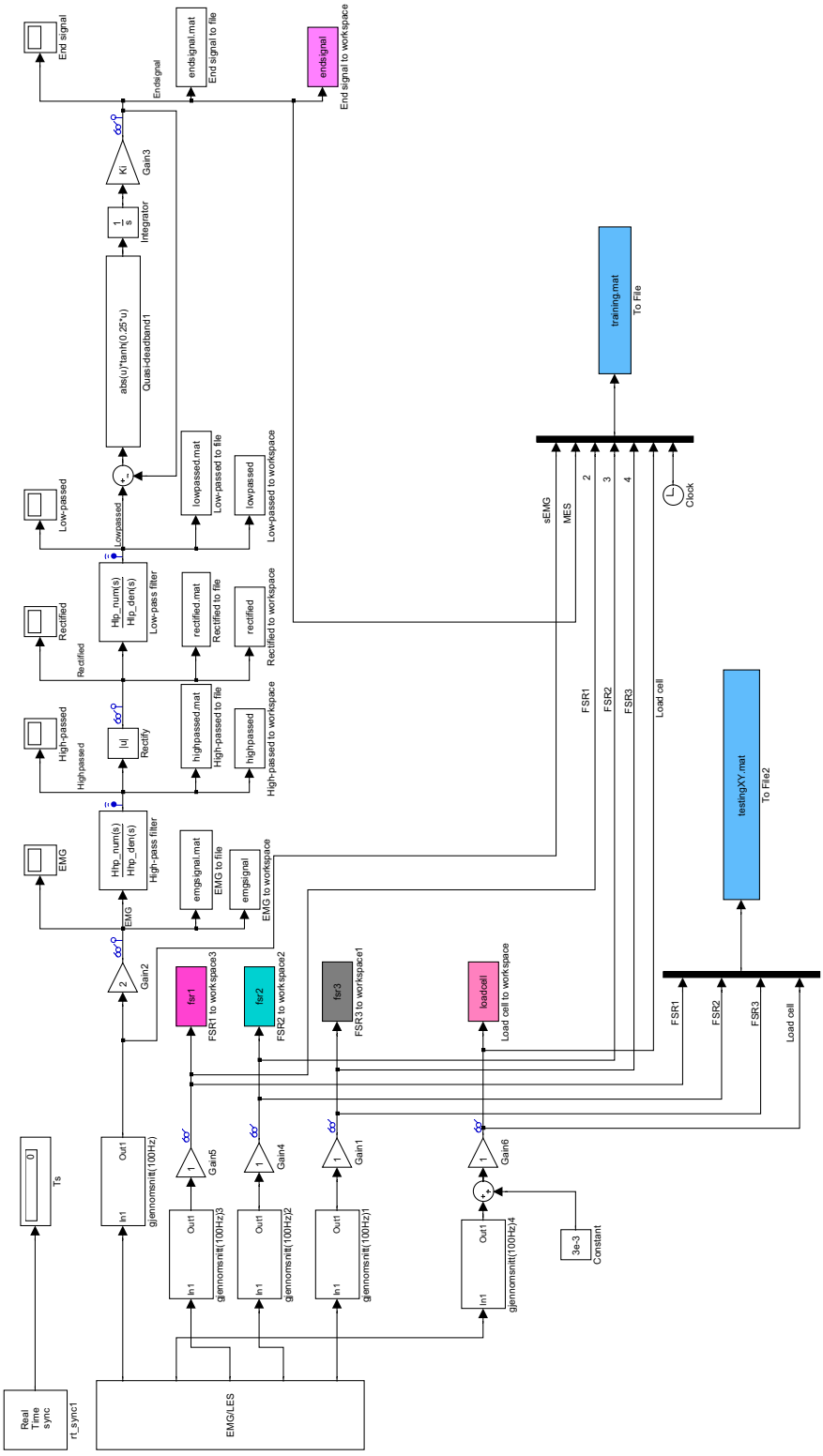

Appendix C Polynomial curve fitting

Appendix C.1 Polynomial curve fitting, 2 degree

See legend in Figure 23 (Section 8).

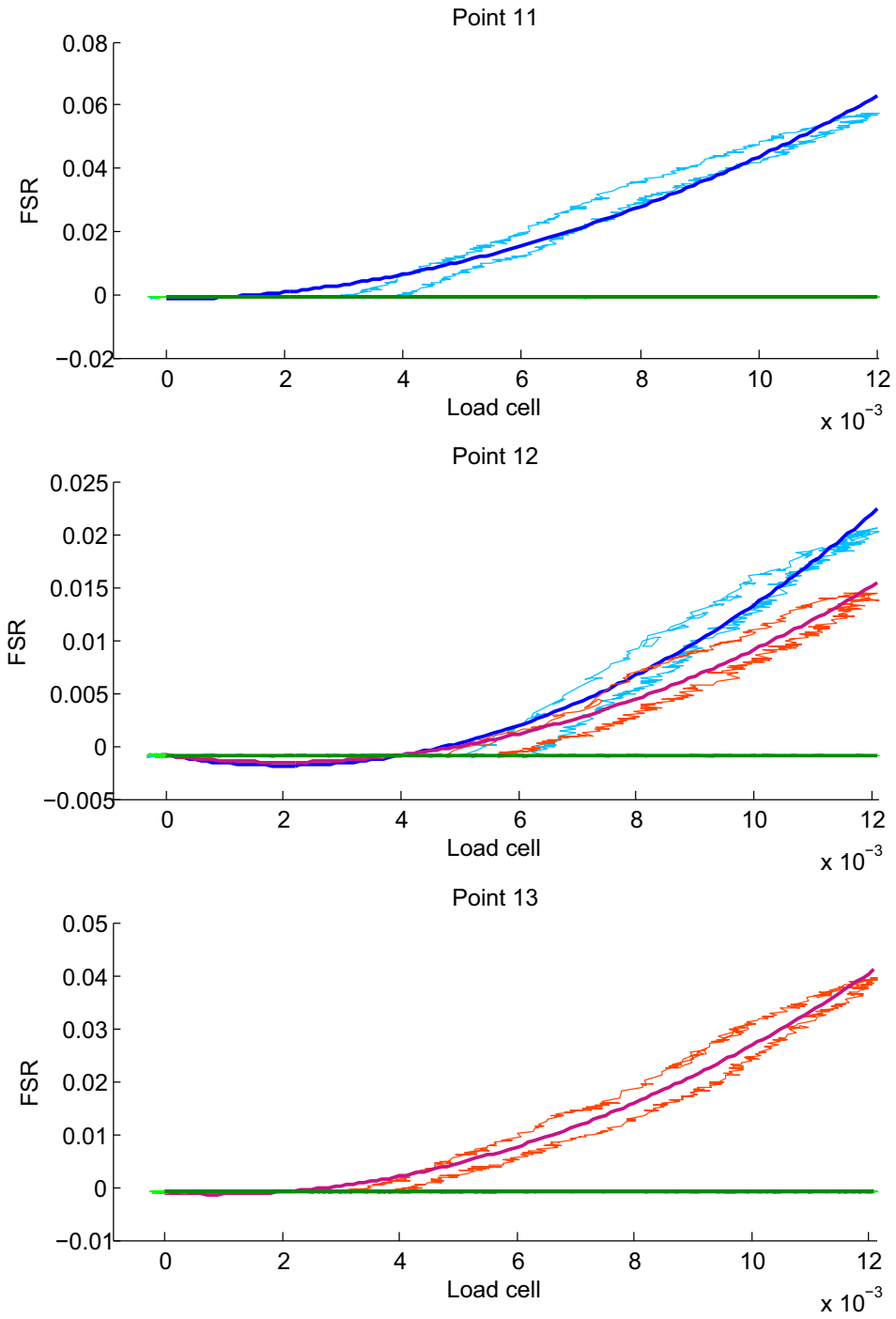

Figure 37: Point 11-12-13, (May 19, 2008)

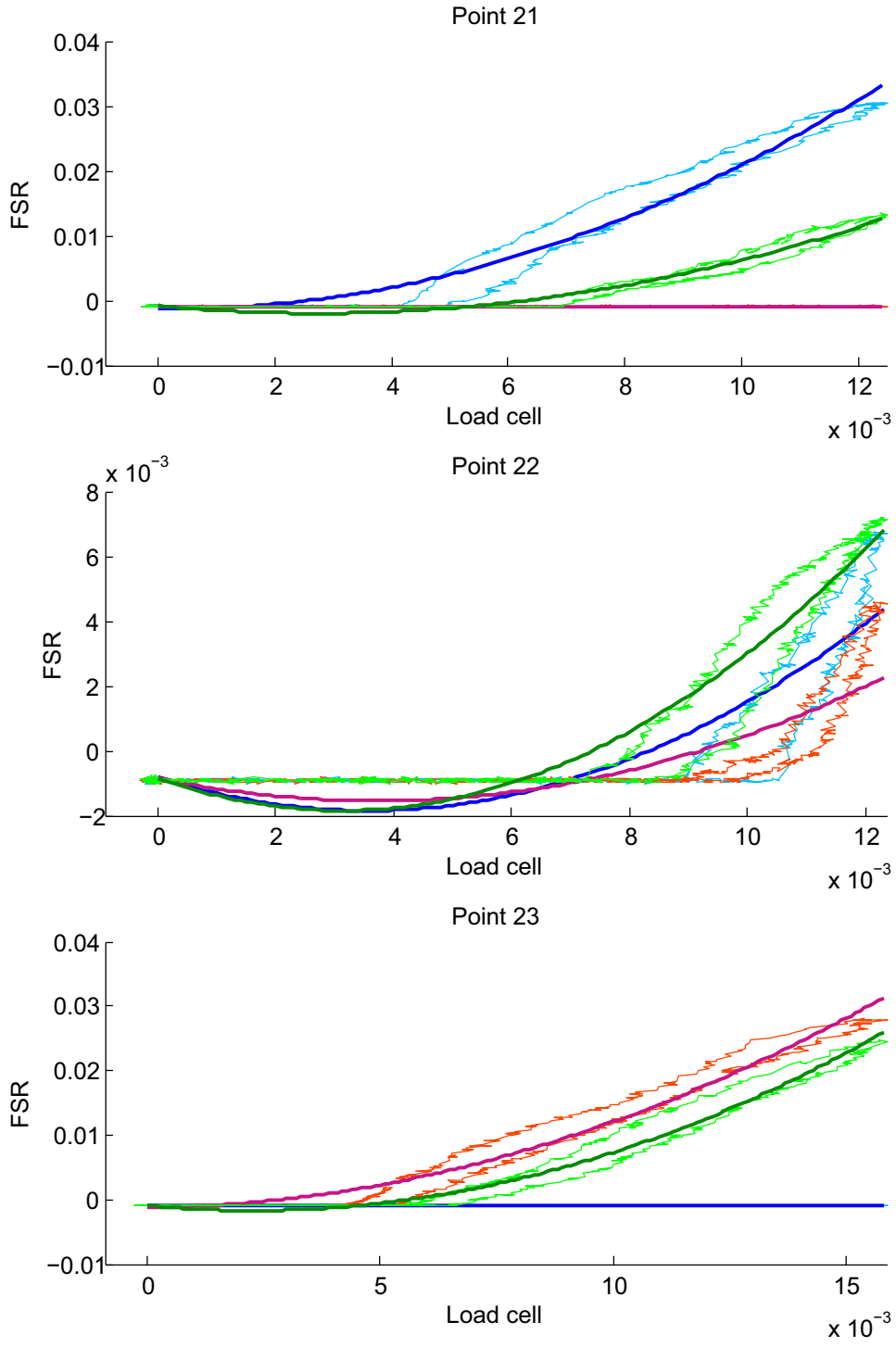

Figure 38: Point 21-22-23, (May 19, 2008)

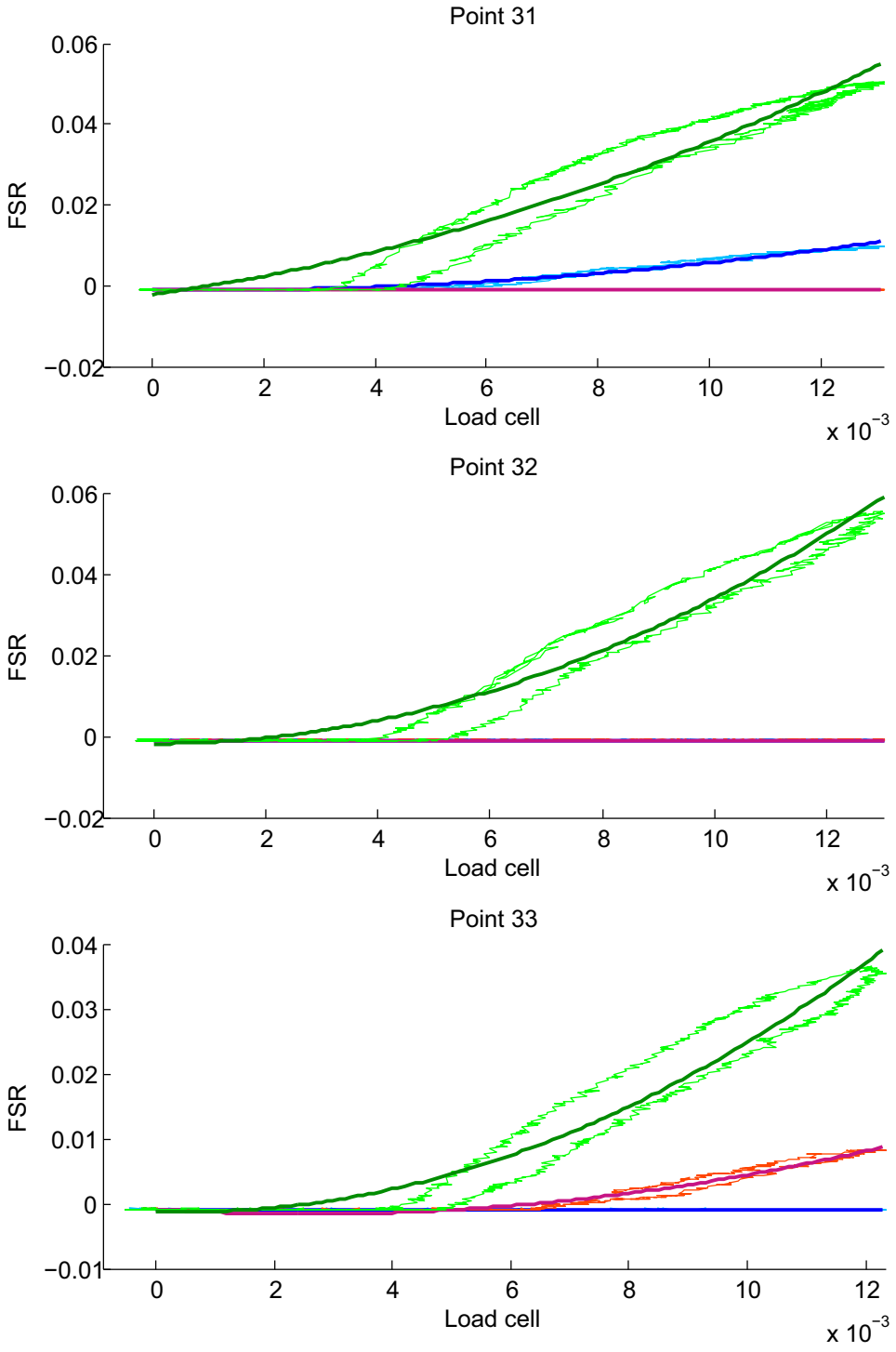

Figure 39: Point 31-32-33, (May 19, 2008)

$$\vec{p}_{11} = \begin{bmatrix} 422.2665 & 0.2916 & -0.0015 \\ 0.0304 & 0.0005 & -0.0009 \\ -0.0932 & 0.0008 & -0.0009 \end{bmatrix} \begin{bmatrix} x^2 \\ x \\ 1 \end{bmatrix} \tag{18}$$

$$\vec{p}_{12} = \begin{bmatrix} 237.3709 & -0.9504 & -0.0009 \\ 164.3983 & -0.6452 & -0.0009 \\ -0.0772 & 0.0010 & -0.0009 \end{bmatrix} \begin{bmatrix} x^2 \\ x \\ 1 \end{bmatrix} \tag{19}$$

$$\vec{p}_{13} = \begin{bmatrix} 0.0831 & -0.0015 & -0.0009 \\ 331.2583 & -0.5236 & -0.0011 \\ -0.0896 & 0.0005 & -0.0009 \end{bmatrix} \begin{bmatrix} x^2 \\ x \\ 1 \end{bmatrix} \tag{20}$$

$$\vec{p}_{21} = \begin{bmatrix} 235.3843 & -0.1330 & -0.0012 \\ 0.0279 & 0.0008 & -0.0009 \\ 155.8694 & -0.8533 & -0.0008 \end{bmatrix} \begin{bmatrix} x^2 \\ x \\ 1 \end{bmatrix} \tag{21}$$

$$\vec{p}_{22} = \begin{bmatrix} 81.1188 & -0.5785 & -0.0008 \\ 51.2701 & -0.3804 & -0.0008 \\ 102.4951 & -0.6401 & -0.0008 \end{bmatrix} \begin{bmatrix} x^2 \\ x \\ 1 \end{bmatrix} \tag{22}$$

$$\vec{p}_{23} = \begin{bmatrix} -0.1172 & 0.0013 & -0.0009 \\ 125.5062 & 0.0777 & -0.0013 \\ 150.7105 & -0.6842 & -0.0009 \end{bmatrix} \begin{bmatrix} x^2 \\ x \\ 1 \end{bmatrix} \tag{23}$$

$$\vec{p}_{31} = \begin{bmatrix} 79.7098 & -0.1301 & -0.0010 \\ 0.0742 & -0.0017 & -0.0009 \\ 189.3894 & 1.8857 & -0.0022 \end{bmatrix} \begin{bmatrix} x^2 \\ x \\ 1 \end{bmatrix} \tag{24}$$

$$\vec{p}_{32} = \begin{bmatrix} -0.2948 & 0.0016 & -0.0009 \\ -0.0519 & -0.0008 & -0.0009 \\ 360.1085 & -0.0108 & -0.0018 \end{bmatrix} \begin{bmatrix} x^2 \\ x \\ 1 \end{bmatrix} \tag{25}$$

$$\vec{p}_{33} = \begin{bmatrix} -0.0534 & -0.0005 & -0.0009 \\ 109.0764 & -0.5609 & -0.0009 \\ 292.5962 & -0.3292 & -0.0011 \end{bmatrix} \begin{bmatrix} x^2 \\ x \\ 1 \end{bmatrix} \tag{26}$$

Appendix C.2 Polynomial curve fitting, 3 degree

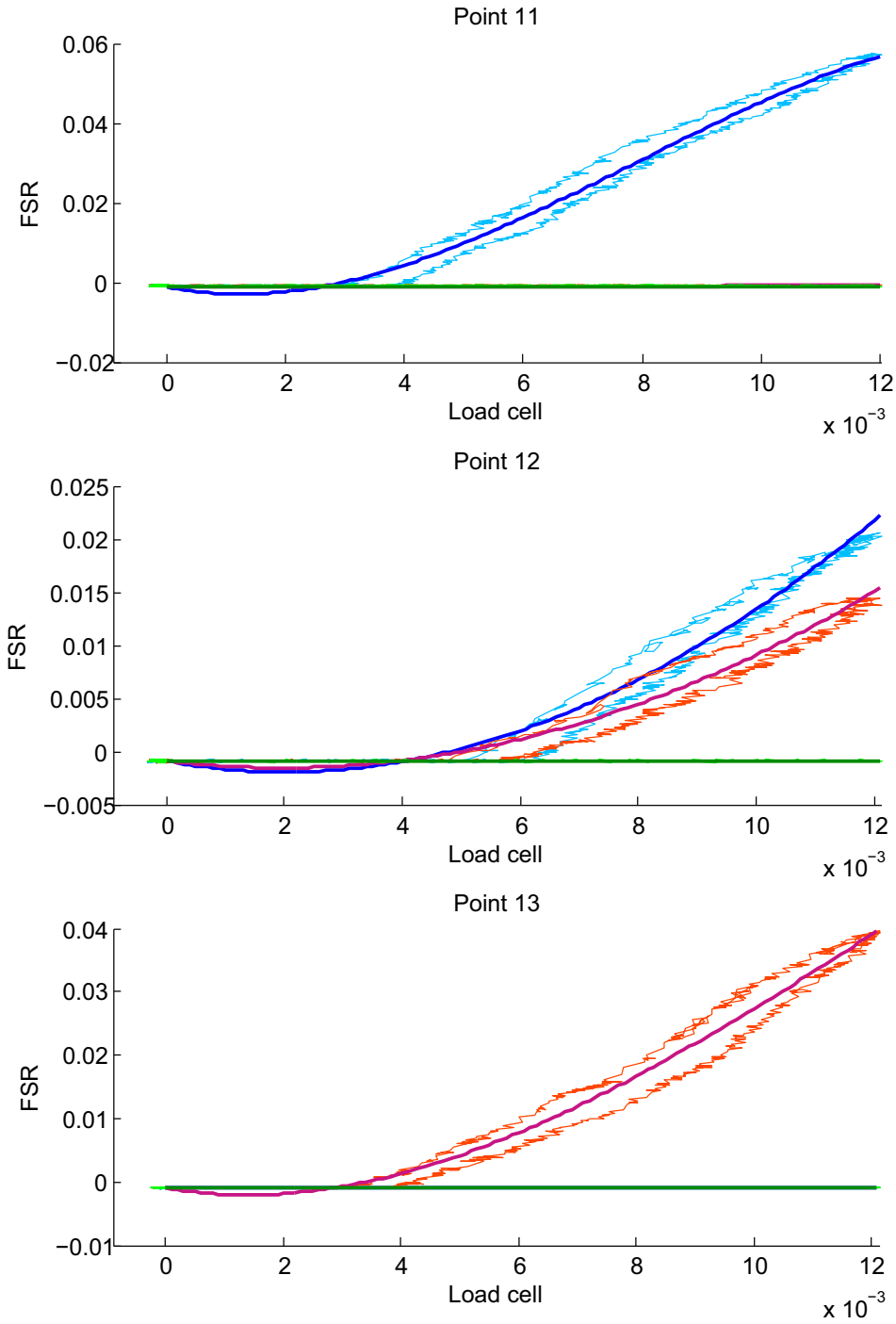

Figure 40: Point 11-12-13, (May 19, 2008)

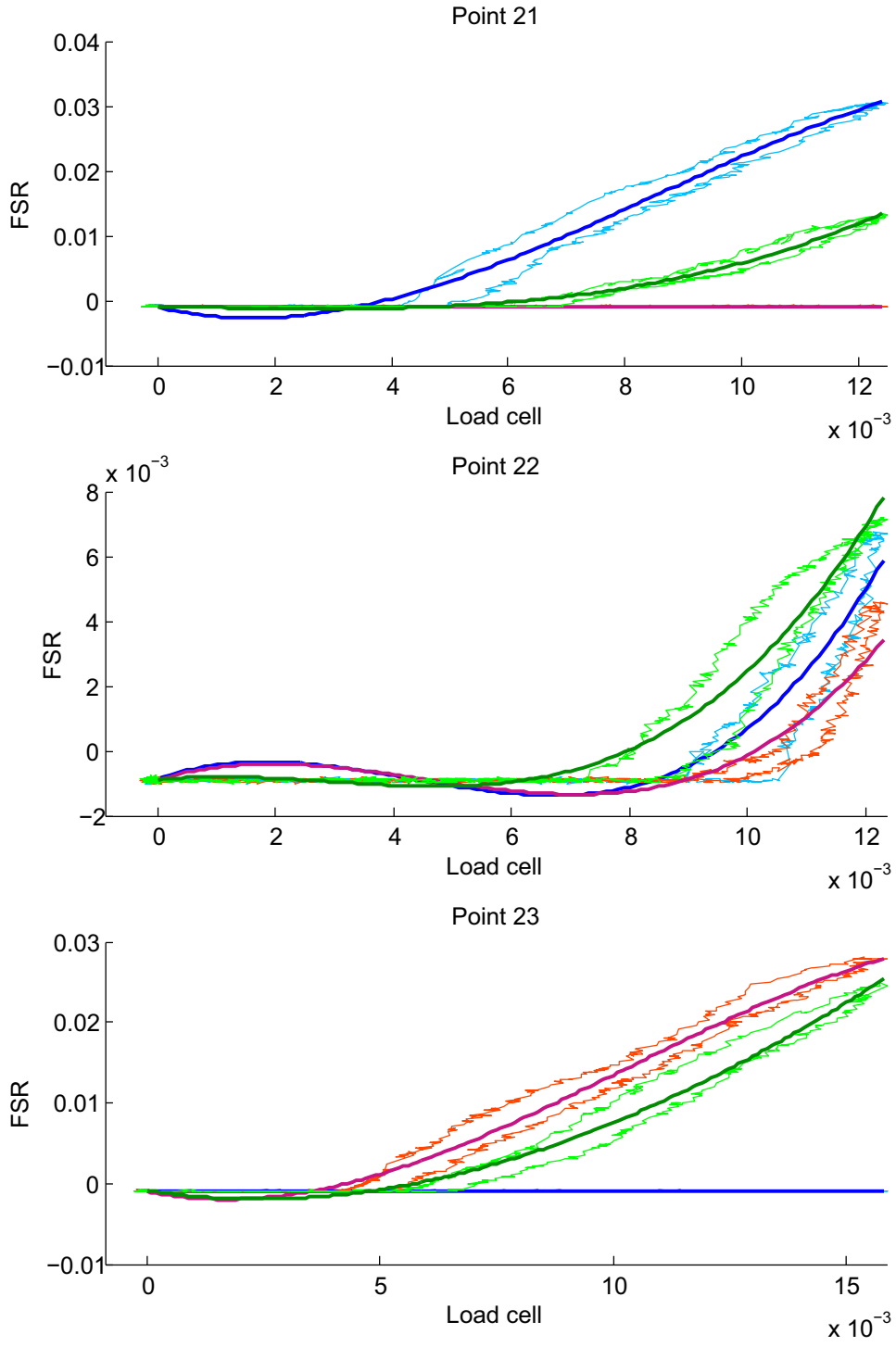

Figure 41: Point 21-22-23, (May 19, 2008)

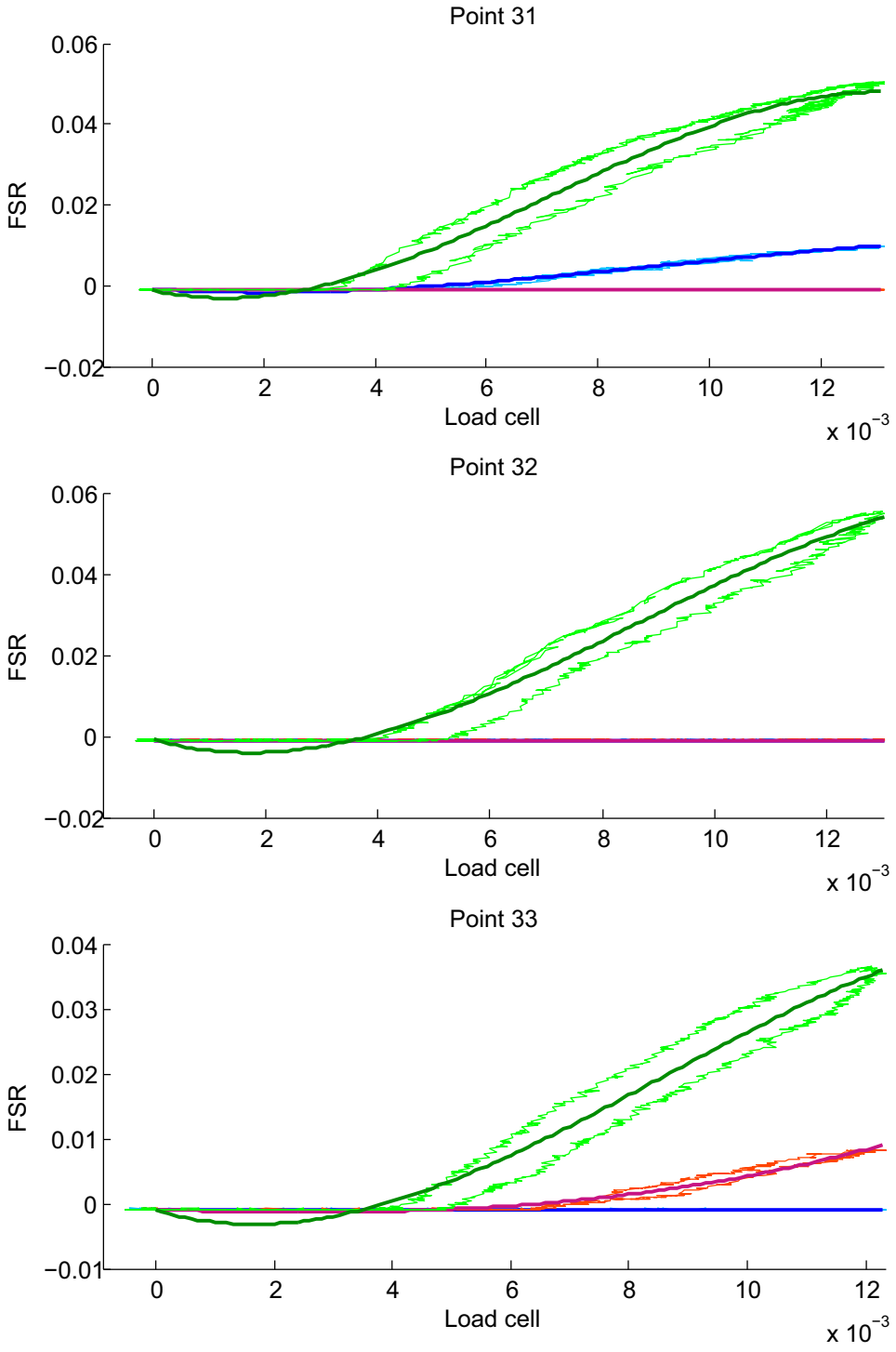

Figure 42: Point 31-32-33, (May 19, 2008)

$$B_{11} = \begin{bmatrix} -56075 & 1333 & -3 & -0.0009 \\ 11.4727 & -0.1558 & 0.0012 & -0.0009 \\ -15.0150 & 0.1505 & -0.0001 & -0.0009 \end{bmatrix} \tag{27}$$

$$B_{12} = \begin{bmatrix} -1501.7 & 262.1 & -1.0 & -0.0009 \\ -74.7008 & 165.6268 & -0.6498 & -0.0009 \\ -36.7229 & 0.5268 & -0.0013 & -0.0009 \end{bmatrix} \tag{28}$$

$$B_{13} = \begin{bmatrix} -34.4532 & 0.6647 & -0.0038 & -0.0009 \\ -16084 & 603 & -2 & -0.0009 \\ -89.3240 & 1.4183 & -0.0054 & -0.0009 \end{bmatrix} \tag{29}$$

$$B_{21} = \begin{bmatrix} -28549 & 734 & -2 & -0.0009 \\ -23.1516 & 0.4327 & -0.0008 & -0.0009 \\ 9129.8 & -3.7 & -0.2 & -0.0009 \end{bmatrix} \tag{30}$$

$$B_{22} = \begin{bmatrix} 17915 & -229 & 1 & -0.0009 \\ 13549 & -183 & 1 & -0.0009 \\ 11824 & -102 & 0 & -0.0009 \end{bmatrix} \tag{31}$$

$$B_{23} = \begin{bmatrix} 3.0936 & -0.1826 & 0.0016 & -0.0009 \\ -12694 & 394 & -1 & -0.0009 \\ -2105.7 & 195.2 & -0.9 & -0.0009 \end{bmatrix} \tag{32}$$

$$B_{31} = \begin{bmatrix} -8961.7 & 245.8 & -0.9 & -0.0009 \\ 0.3079 & 0.0685 & -0.0017 & -0.0009 \\ 62517 & 1348 & -3 & -0.0009 \end{bmatrix} \tag{33}$$

$$B_{32} = \begin{bmatrix} 24.8791 & -0.7521 & 0.0036 & -0.0009 \\ 7.5626 & -0.1909 & -0.0002 & -0.0009 \\ -48397 & 1250 & -4 & -0.0009 \end{bmatrix} \tag{34}$$

$$B_{33} = \begin{bmatrix} 48.4649 & -0.8837 & 0.0028 & -0.0009 \\ 957.1 & 41.3 & -0.3 & -0.0009 \\ -34077 & 876 & -3 & -0.0009 \end{bmatrix} \tag{35}$$

Appendix D Results, MLP network

Legend in section 8.2.1.

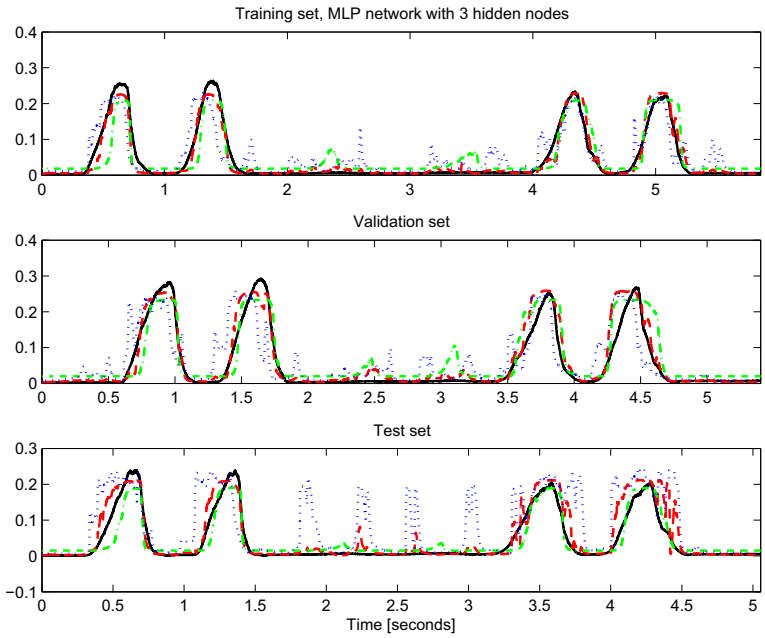

Figure 43: MLP network with 3 hidden nodes

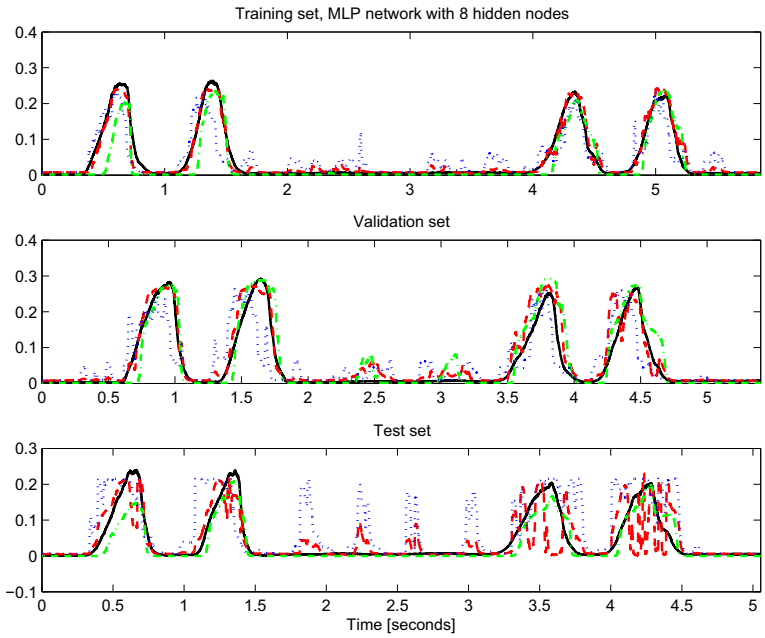

Figure 44: MLP network with 8 hidden nodes

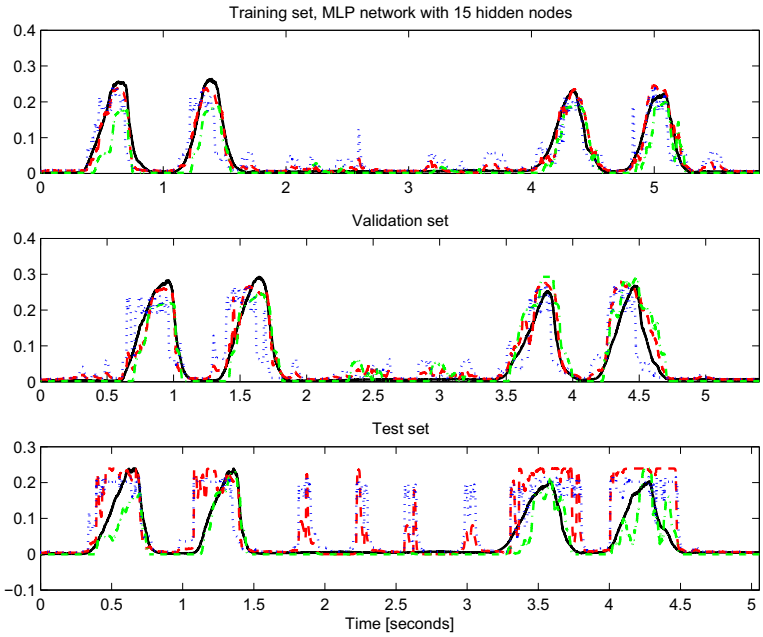

Figure 45: MLP network with 15 hidden nodes

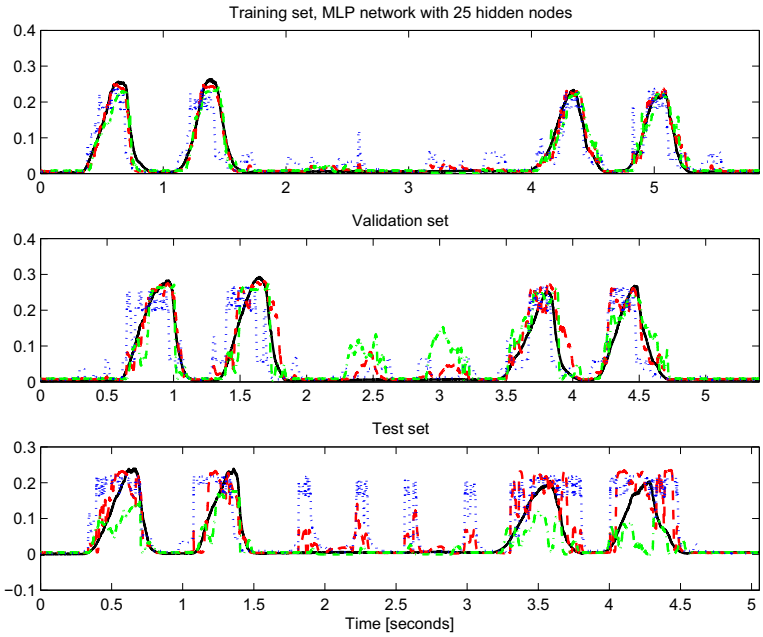

Figure 46: MLP network with 25 hidden nodes

Appendix E CD

Here is a short explanation of what is put on the CD.

E.1 Report Contains the Master's thesis as a PDF file, and a subfolder with LaTeX source code.

E.2 References Contains some of the references as PDF files.

E.3 LaboratoryWork Contains files from the laboratory.